EFFECT OF FLUID'S REYNOLDS NUMBER AND SPACER FILAMENTS FLOW ATTACK ANGLE IN SPACER-FILLED CHANNEL

LEE JIAN

UNIVERSITI TUNKU ABDUL RAHMAN

EFFECT OF FLUID'S REYNOLDS NUMBER AND SPACER FILAMENTS FLOW ATTACK ANGLE IN SPACER-FILLED CHANNEL

LEE JIAN

A project report submitted in partial fulfilment of the requirements for the award of Bachelor of Engineering (Hons.) Chemical Engineering

Lee Kong Chian Faculty of Engineering and Science
Universiti Tunku Abdul Rahman

April 2015

DECLARATION

I hereby declare that this project report is based on my original work except for citations and quotations which have been duly acknowledged. I also declare that it has not been previously and concurrently submitted for any other degree or award at UTAR or other institutions.

Signature : _____

Name : Lee Jian

ID No. : 11UEB02057

Date : 13 April 2015

APPROVAL FOR SUBMISSION

I certify that this project report entitled **"EFFECT OF FLUID'S REYNOLDS NUMBER AND SPACER FILAMENTS FLOW ATTACK ANGLE IN SPACER-FILLED CHANNEL"** was prepared by **LEE JIAN** has met the required standard for submission in partial fulfilment of the requirements for the award of Bachelor of Engineering (Hons.) Chemical Engineering at Universiti Tunku Abdul Rahman.

Approved by,

Signature : _____

Supervisor : Ir. Teoh Hui Chieh

Date : 13 April 2015

Specially dedicated to
my beloved mother and father.

ACKNOWLEDGEMENTS

I would like to thank everyone who had contributed to the successful completion of this project. I would like to express my gratitude to my research supervisor, Ir. Teoh Hui Chieh for her invaluable advice, guidance and enormous patience throughout the development of the research.

In addition, I would also like to express my gratitude to my loving parent and friends who had helped and given me encouragement throughout the performance of this project.

EFFECT OF FLUID'S REYNOLDS NUMBER AND SPACER FILAMENTS FLOW ATTACK ANGLE IN SPACER-FILLED CHANNEL

ABSTRACT

Fouling and concentration polarisation are two major problems that are often associated with spiral wound membrane (SWM) modules. In order to reduce and attempt to mitigate said problems, turbulence can be induced in the feed flow through the usage of spacers, a rigid net-like structure placed between two membrane leaves in a SWM module. Besides creating turbulence by promoting the formation of vortices and eddies in the feed flow, the pressure drop across the module has to be minimised to maintain effective permeation across the membrane. Furthermore, a considerable amount of shear stress has to be provided on the top and bottom surface of the membrane in order dislodge deposited particles which causes potential membrane fouling. All these parameters analysed and monitored by simulating a 3D spacer-filled channel using ANSYS Fluent v15, a commercial computational fluid dynamics (CFD) solver that is able to precisely model flow patterns and conditions in a wide range of geometries. In this study, fluid with varying Reynolds number in the range of 100 to 500 is allowed to flow through a spacer-filled channel with varying flow attack angles. The optimal Reynolds number and flow attack angle were judged based on their fluid velocity trends, pressure drop across the spacer-filled channel, magnitude of wall shear stress as well as the formation of vortices and eddies in the flow patterns. Based on this study, it was found that fluid must possess a Reynolds number of greater than 200 in order to exhibit significant and reasonable magnitudes of wall shear stress as well as eddies and vortices. Also, it was found that spacer filaments arranged in a 45° flow attack angle was optimal despite having a considerably large pressure drop.

TABLE OF CONTENTS

LIST OF TABLES

LIST OF FIGURES

LIST OF SYMBOLS / ABBREVIATIONS

D_o	spacer filament outer diameter
D_i	spacer filament inner diameter
h	channel height
T	temperature, K
V	mean fluid velocity
W	twist pitch
α	mesh angle
β	flow attack angle
ρ	fluid density
μ	fluid viscosity
CFD	computational fluid dynamics
MF	modified filaments
PRESTO!	pressure staggering option
SIMPLE	semi-implicit method for pressure-linked equations
SWM	spiral wound membrane
TT	twisted tape
URF	under relaxation factor

CHAPTER 1

INTRODUCTION

1.1 Background

The term membrane refers to a structure with a thickness much smaller than its other dimensions that allows for mass transfer through it (Koros, Ma and Shimidzu, 1996). In membrane technology, a bulk fluid mixture known as the feed will come in contact with the membrane and attempt to diffuse through it. Materials or substances that are able to pass through the membrane are termed as permeate while those that are not are known as retentate or raffinate. Membrane separation processes can be classified using two main methods i.e. by their selectivity which depends on the size of the pores or by their membrane modules. Today, separation processes using membranes grouped by their pore sizes generally fall into four different categories which are, in order of decreasing pore size and increasing selectivity, conventional filtration, microfiltration (MF), ultrafiltration (UF), nanofiltration (NF) and reverse osmosis (RO) (Nath, 2008). Figure 1.1 shows the selectivity of membranes and the relative particle diameters.

In practice, to increase the efficiency and effectiveness of membrane separation processes, membranes are designed and arranged into the form of modules. Today, prominent modules of membrane processes include the plate-and-frame module, tubular module, spiral wound module and hollow fibre module (Baker, 2004). Membrane separation processes are particularly advantageous over other separation processes as most of them does not require a change in the phase of the feed thus causing a significantly lower energy consumption. Also, the flow sheet of

membrane processes are relatively simpler and simultaneously provides incredible selectivity in separation.

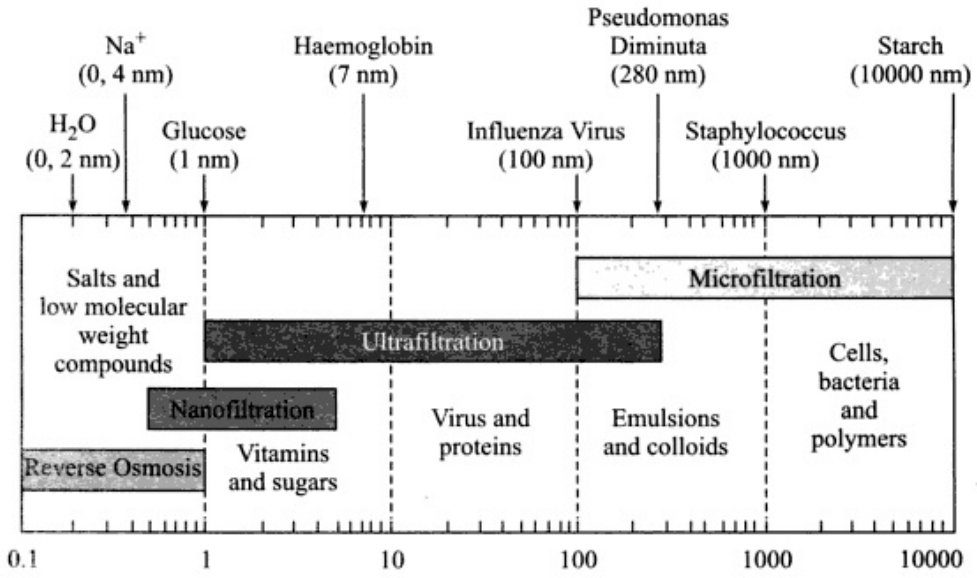

Figure 1.1: Membrane Selectivity based on Particle and Pore Sizes (Nath, 2008)

1.2 Spiral Wound Membrane (SWM)

A spiral wound membrane (SWM) is a type of membrane module consisting of essentially a rolled up version of a flat sheet membrane combined with feed spacers and permeated carriers layered on the top and bottom layers of the membrane. Like any other membrane configurations, there are three types of streams flowing into and out of the membrane module namely the feed, permeate and retentate or raffinate. Figure 1.2 illustrates the typical components found in a SWM and the direction of the permeate flow.

In a SWM, the feed enters the membrane from one end at multiple points between the layers of the spiral while the retentate exits the module at the other end in a similar fashion. Inside the module, the feed will travel from the outer layers of the module towards the core of the spiral where the permeate is collected. In doing so, the feed inside the membrane flows in three different ways namely axial flow, which

refers to the flow parallel to the respective surfaces of the membrane, transverse flow which represents the flow of feed solution inwards towards the core through the multiple layers of the spiral and lastly spiral flow which is the flow along the spiral pathway of the membrane. Present between the layers of the membrane are net-like structures known as spacers which mainly act as a support to create space for flow throughout the module. Besides that, there is also a layer known as the permeate collection material or permeate carrier which facilitates the transport of permeate toward the core.

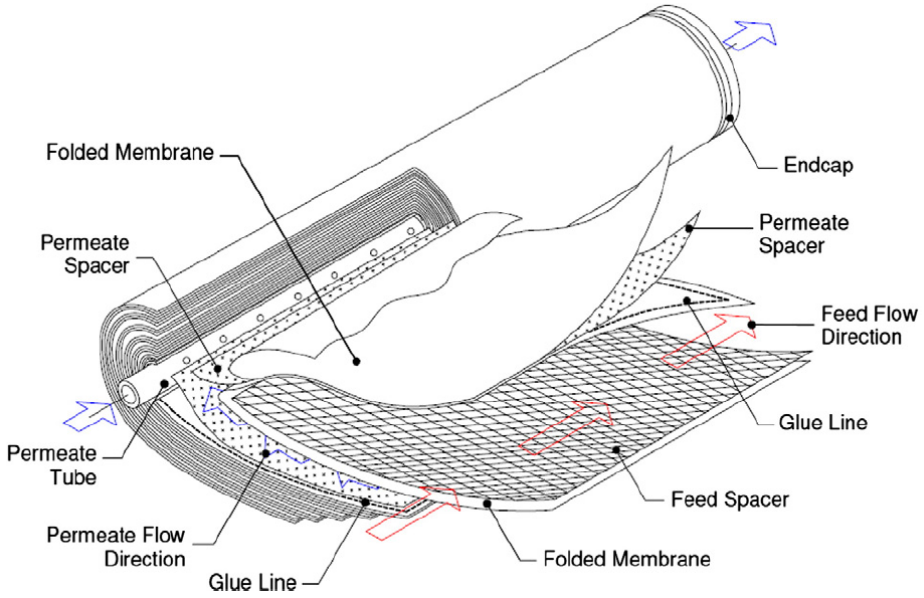

Figure 1.2: Configuration of a Spiral Wound Membrane (Karabelas, Kostoglou and Koutsou, 2015)

In part with the aim of optimising membrane modules, it is important to determine the behaviour of parameters such as pressure drop, mass transfer and flow turbulence in the module. One method used in achieving this aim is to analyse the hydrodynamics of flow patterns in the module. The flow patterns within the membrane module environment can be simulated and analysed using computational fluid dynamics (CFD) modelling and simulation techniques. This involves obtaining solutions to the Navier-Stokes equation using numerical methods. Using ANSYS, a simulated environment can be created and parameters such as the membrane and spacer geometry, flow velocity, pressure drop and feed components can be adjusted and visualised to obtain valuable data on the flow patterns within the SWM.

1.3 Problem Statement

One of the main problems encountered in membrane modules is fouling. Koros, Ma and Shimidzu (1996) defined the term fouling as a process that causes a loss in the performance of a membrane due to the suspended or dissolved substances deposited on its external surfaces, at its pore openings or within its pores. Realistically, not all substances that fail to pass through the membrane layer will pass out as retentates. Small amounts of such substances will be lodged and stuck in various parts of the SWM and build up over time. Furthermore, the feed solution is seldom void of impurities which could be damaging or corrosive to the membrane. This reduces the filtration efficiency as well as the life of the membrane.

Another problem often encountered in membrane related processes is concentration polarization. Koros, Ma and Shimidzu (1996) also provided a definition for this term which is a concentration profile with a higher level of solute near the upstream membrane surface to the well mixed bulk fluid far from the membrane surface. Generally, concentration polarisation occurs due to the selectivity in permeation of certain components in the feed by the membrane causing a difference in the rate of permeation of different components in the feed. Consequently, components that are permeated slower will accumulate on the surface of the membrane on the feed side while components that permeates faster will be concentrated on the permeate side of the membrane. As a result, a concentration gradient is created across the membrane and the diffusion flux and membrane selectivity is reduced.

Since both of these problems are essentially caused by the deposition of particles on the surface of the membrane, one approach in rectifying this is by using the spacers located between the layers of membrane to induce turbulence in the flow within. Turbulence brings about high shear force which can dislodge deposited particles and effectively improve the efficiency and life of SWM. With respect to the spacers, the magnitude of turbulence induced by the spacers depends very much on factors such as the shape and geometry of the spacers, the attack angle of the feed, distance between lengths of filament and size of the filaments.

1.4 Aims and Objectives

As briefly mentioned in the previous section, this report aims to study the effectiveness in the usage of spacers to induce turbulence in the flow within the spacer-filled feed channel of a SWM module. CFD modelling and simulation of the flow within the channel is carried out using ANSYS Fluent v15. In particular, the desired parameters to be studied are the fluid's Reynolds number as well as the flow attack angle on the feed spacers. These parameters will be varied within a certain range and the effects on the fluid velocity, pressure drop across the channel module as well as the formation of vortices will be analysed.

1.5 Scope of Study

Due to the complex design of a SWM module, this study will not design, model and simulate the flow occurring in the entire membrane module. Instead, the study will focus on the flow in a small and arbitrary section of a single feed spacer-filled channel of the module. In addition, the curvature of the channel is also neglected as the dimensions of the channel are relatively smaller than the entire SWM module and thus assumed to be flat. It is also important to note that the study assumes that the properties of the membrane layer of the module does not have any major effect on the bulk flow of the fluid in the spacer feed channel and thus will not be included in the simulation environment. This assumption was also made by Lau, et al. (2009) who found that the permeating flux was significantly smaller than the feed inlet velocity and hence did not drastically affect the velocity profile of the flow generated.

CHAPTER 2

LITERATURE REVIEW

2.1 Feed Spacers

In a spiral wound membrane, the several sheets of membrane leaves are wound together around a core which collects the permeate of the module. Without a layer of material sandwiched between the layers of membranes, the membrane module will be extensively soft and thus unable to support itself well. Besides, feed flowing into the module will not be able to efficiently pass through the layers of the membrane due to the absence of spaces between them. Hence, a rigid net-like structure known as feed spacers is placed between the membrane layers and thus creating a channel for the feed flow as well as acting as a support for the module. Li, et al., (2002a) stated that the feed spacer provides mechanical support between the membrane leaves while promoting the formation of vortices in the feed flow regime. Typically, research and studies on feed spacers involves changing and optimising the design of the feed spacers in terms of spacer filaments shapes and geometry, mesh length ratio, crossing angle or mesh angle and feed attack angle (Ahmad, Lau and Abu Bakar, 2005; Lau, et al., 2009; Lau, et al., 2010). The feed spacers can then be evaluated on its efficiency and effectiveness in terms of factors such as, pressure drop, specific power consumption, concentration polarization factor and mass transfer through Sherwood number (Lau, et al., 2010; Li, et al., 2002a).

2.2 CFD Modelling of Feed Spacer Filled Channels

Due to the growing interest in the flow patterns induced by feed spacers, a significant amount of research papers have been published on the modelling of the flow in a spacer filled channel which can be used to predict and estimate the actual flow patterns in a SWM module. CFD is a numerical technique commonly utilised to model the flow conditions in a feed spacer filled channels. One advantage possessed by computational and numerical techniques over the conventional experimental techniques is the capability to obtain information on the flow conditions at any point in the geometry without interrupting the flow. Also, the results obtained through computational modelling can be easily replicable which saves time and cost compared to experimental setups which can be expensive and costly (Fimbres-Weihs and Wiley, 2010). However, the accuracy of computational data has to be verified as it depends very much on the setup of the model. Thus, a mesh independence test is often carried out in order to verify that effects of the mesh quality on the results obtained is small and negligible. Furthermore, a validation of the computational results should be validated experimentally to check the reasonability of the results.

2.3 Variations in Feed Spacer Channels

In CFD modelling, a larger variety of design of feed spacers and feed spacer channels can be tested at ease as geometries can be easily sketched and drawn. This process can be tedious and costly as the spacer filaments have to be physically fabricated along with the channel. Furthermore, the fabrication of spacer filaments is limited to the fabrication technology and may not be able to fabricate novel shapes and geometry that are not commercially available. Typical parameters tested in CFD modelling of feed spacer channels include the spacer filaments shape and geometry, spacer mesh length ratio, feed attack angle, and filament crossing angle.

2.3.1 Spacer Filaments Shape and Geometry

One way spacer filaments can be different from each other is to have different shape and geometry such as cylinder, rectangular (cuboidal), triangular (prism) as well as other unique and novel geometries such as a concave cylinder and a spiralling cylinder. Conventional filaments, which are cylindrical in shape can be regularly arranged in a non-woven manner or woven as shown by Li, et al. (2002a). Other shapes and geometries will be discussed in the following sections.

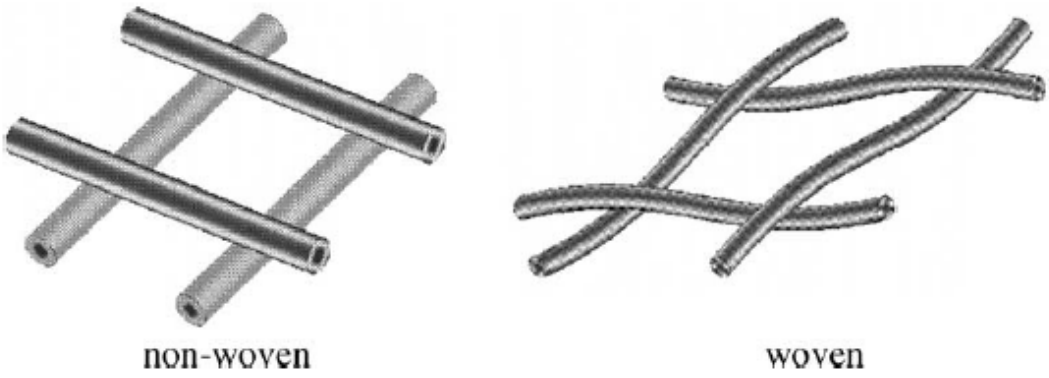

Figure 2.1: The Basic Shapes of Commercial Net Spacers (Li, et al., 2002a)

Ahmad, Lau and Abu Bakar (2005) conducted a study on the effect of different geometrical shapes of spacer filaments in terms of concentration factor, turbulent intensity and pressure drop using a feed of NaCl solution of varying Reynolds number in the range of 400 to 1000. Three geometrical shapes of filaments were tested which are the circular, square and triangular filaments all with a filament height of 0.5 mm and arranged on a single layer with a mesh length ratio of 4. Figure 2.2 shows the design of the spacer filaments tested. As a result, it was found that triangular filaments showed the best performance in terms of high turbulent intensity and low concentration factor with minimal pressure drop. However it was also highlighted by Ahmad, Lau and Abu Bakar (2005) that spacers with triangular filaments are impractical in terms of fabrication and may not be available in the market. Furthermore, the study was done using a 2D simulation which results may not be fully applicable to the actual 3D flow patterns in a real spacer filled channel. Not to mention, the study did not vary the mesh length ratio of the filaments which may yield different results.

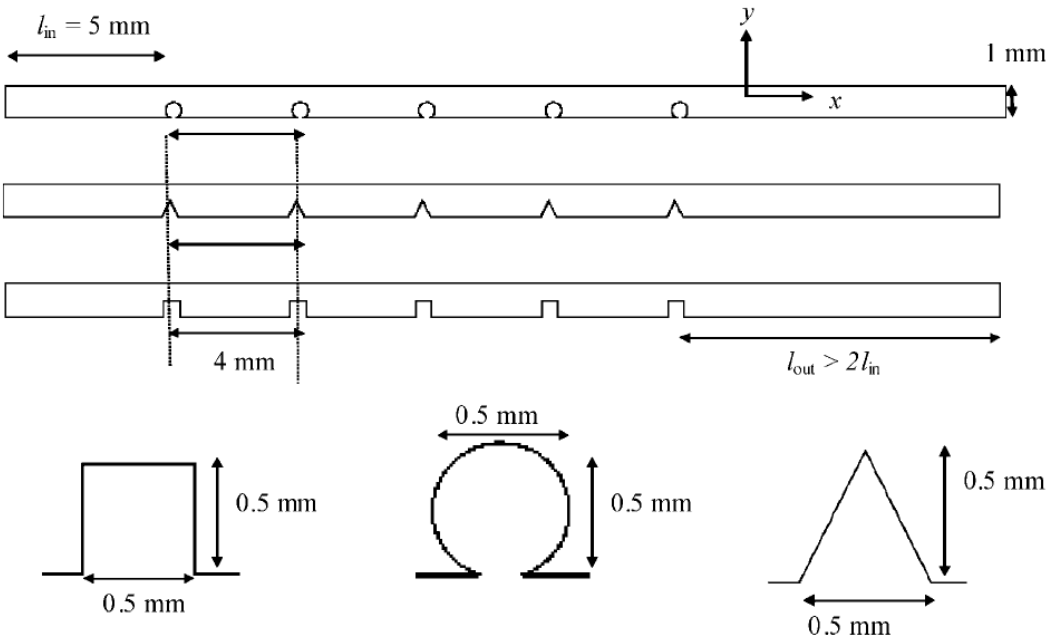

Figure 2.2: 2D Spacer Filaments of Different Geometries (Ahmad, Lau and Abu Bakar, 2005)

Dendukuri, Karode and Kumar (2005) proposed new designs for spacers which are concave in shape compared to the convex cylindrical shape as shown in Figure 2.3. The convex shape of the spacers allow for more variations in the geometry of the filaments as it can utilise the independence of the diameter of the convex region and the width and height of the filaments. Cylindrical spacers on the other hand can only be different in terms of diameter. The setup of 3D model used in the study was not explicitly mentioned. However, it is assumed that the specifications of the spacers used such as the mesh angle or hydrodynamic angle as described in the study and other dimensions were based on the commercial spacers Conwed-1, UF-2 and Naltex-56 since the results obtained are compared to the aforementioned commercial spacers. The results showed significant reduction in pressure drop when tested a feed of water of inlet velocities between 0.25 to 1.0 m/s in all the proposed design. Besides that, the strain rates maintained by the proposed design were also comparable to the commercial spacers. Similar to the case studied by Lau, Ahmad and Abu Bakar (2005), the proposed designs are not available in the market and hence experimental results could not be obtained to validate the simulated conditions. However, this showed that there ample research potential in using different shapes and geometry in the optimisation of feed spacers.

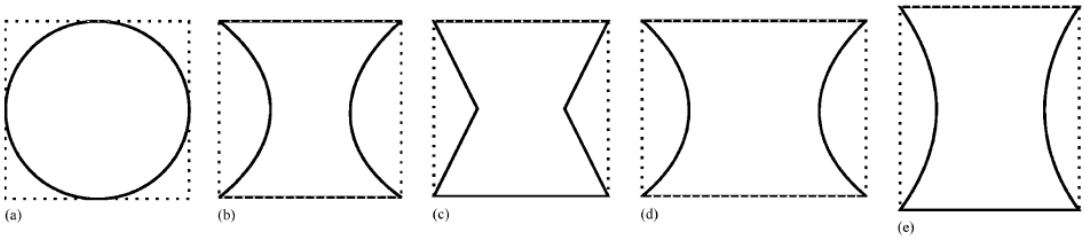

Figure 2.3: Cross Sections of Spacer Filaments (a) Original Spacer (b) Concave (squire) (c) Rectangular (vertical) (d) rectangular (w/h = 4/3) and (e) rectangular (w/h = 3/4) (Dendukuri, Karode and Kumar, 2005)

Other interesting geometrical configuration of spacer filaments include the ladder-type spacers, staggered herringbone spacers and helical spacers. Ladder-type spacers are made of cuboidal filaments arranged in a uniform pattern. Staggered herringbone spacers are made by arranging the cuboidal filaments in an asymmetric manner as shown in figure 2.4. Helical spacers are made up of thin plates twisted into a helical shape. Shrivastava, Kumar and Cussler (2008) studied the effectiveness of the aforementioned spacers by measuring the mass transfer occurring in a spacer filled channel through the measurement of the limiting current density of the flow. According to the study, there is a significant increase in the mass transfer induced by the staggered herringbone spacers and the helical spacers. This is favourable as a high value of mass transfer likely indicates low concentration polarisation factor. However, there are limitations to the results of the study as well as pointed out by Shrivastava, Kumar and Cussler (2008). Firstly, the increase in mass transfer typically comes with an increase in pressure drop. Also, the results may not be relatable in membrane modules as there are flow processes compared to the study which models the mass transfer as a diffusion process. Nevertheless, these spacers are novel models and prove that spacer shapes and geometry does play a major role in affecting flow patterns.

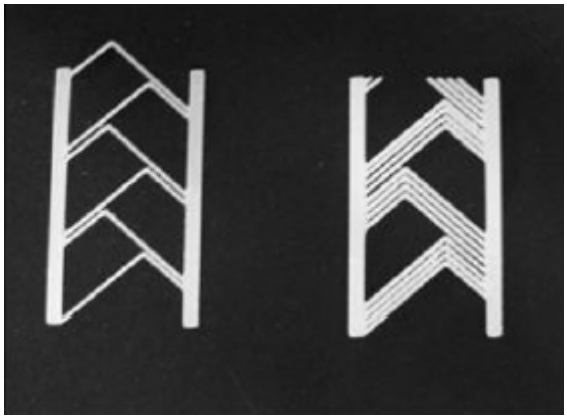

Figure 2.4: Staggered Herringbone Spacers (Shrivastava, Kumar and Cussler, 2008)

Similar spacer filament geometries were also studied by Li, et al., (2005) in hopes of generating an optimal flow patterns with both longitudinal and transversal vortices in order to enhance the mass transfer efficiency. The first spacer geometry studied is known as a modified filament (MF) which consists of conventional cylindrical spacers filaments modified by winding a rod helically around the spacer filaments. The second spacer geometry is a twisted tape (TT) which is a rectangular tape twisted helically. Also tested are multi-layer spacers with twisted tapes (MLTT) and multi-layer spacers with normal filaments (MLNF) which consists of an additional layer of cylindrical filaments of 1 mm and a mesh length ratio of four. The study is done experimentally due to the complex configuration of the spacer filled channel which makes CFD modelling unreliable (Li, et al., 2005). Hence, the spacers are fabricated to yield a feed attack angle, α of 45° and a mesh angle, β of 90°. Among the dimensions of the spacers noted include the 360° twist pitch, W, channel height, h, the modified filament's inner and outer diameter, D_i and D_o respectively as well as the thickness of the tape, t. The mesh length ratio, l/h as well as dimensionless parameters D/h, D_i/h and D_o/h are computed. The values of the parameters used are summarised in table 2.1 while detailed illustrations of the spacer filaments studied can be found in figures 2.5 and 2.6.

Table 2.1: Geometric Parameters of MF and TT Spacers (Li, et al., 2005)

	h (mm)	l/h	α (°)	β (°)	W/h	D/h	D_i/h	D_o/h	t/h
MF	4	4	45	90	2	-	0.34	0.50	0.13
TT	4	4	45	90	1	0.50	-	-	0.13

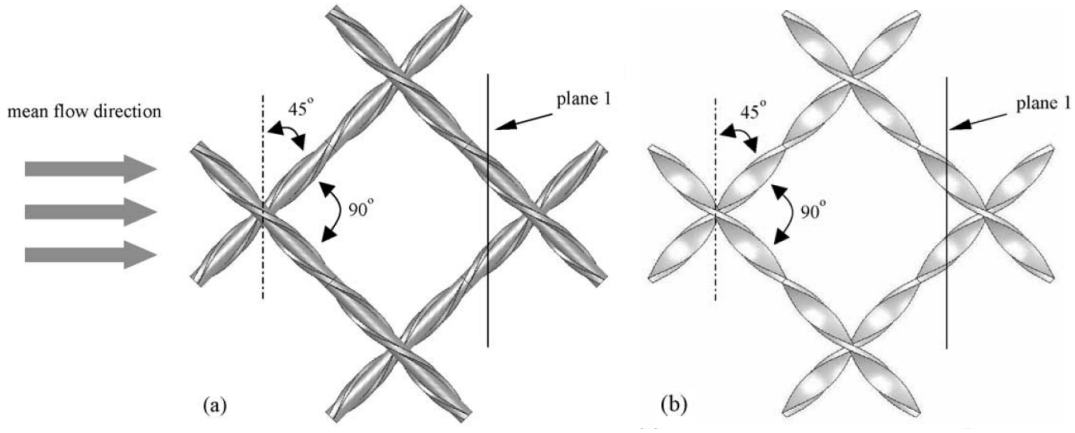

Figure 2.5: Spacer Filaments Arrangement and Orientation (Li, et al., 2005)

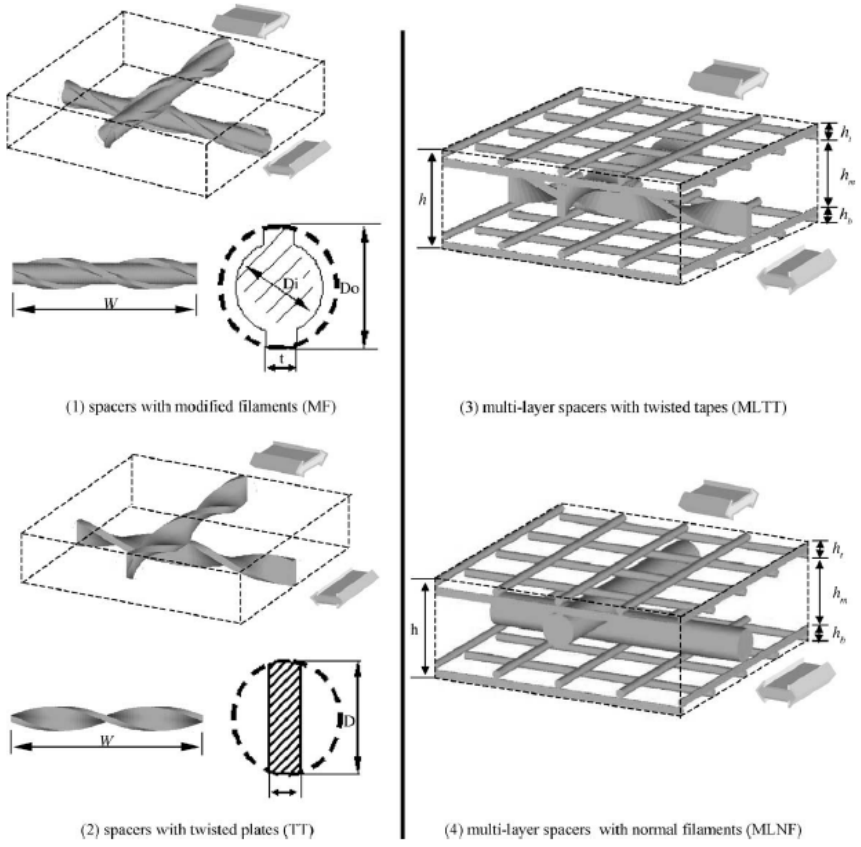

Figure 2.6: Spacer Filaments' Measured Dimensions (Li, et al., 2005)

The study found that the performance of MF and TT spacers are both inferior to the conventional non-woven cylindrical spacer filaments. This is because the flow generated largely consists of longitudinal vortices which does not contribute to the enhancement of mass transfer. However, the MLTT spacer showed promising results due to the lower power dissipation near the twisted tape spacers found in the middle layer. Also, the average value of the Sherwood number, a dimensionless parameter that is directly proportional to the mass transfer coefficient is at least 30% higher in MLTT spacers compared to the conventional cylindrical non-woven spacers. The main drawback of MLTT spacer is complexity of its design which makes it costly and difficult if not impossible to fabricate commercially.

2.3.2 Mesh Length Ratio, Mesh Angle and Feed Attack Angle

Lau, et al. (2010) simulated a two dimensional flow using a channel of 1 mm in height and non-woven single layer cylindrical spacer filaments with a diameter of 0.5 mm arranged at variable distances apart using a $CuSO_4$ solution as a feed with Reynolds number between 200 to 700. It was found that the single layer spacer arranged with a mesh length ratio of three i.e. the filaments are arranged with a distance of 3 mm apart produces the lowest effective concentration polarisation factor at the lowest specific power consumption. However, feed spacers with mesh length ratio of three does not handle feed with high Reynolds number well as the rate of increase in specific power consumption with increasing feed Reynolds number is the largest compared to other mesh length ratio. Consequently, the rate of increase in pressure drop is also the highest with increasing feed Reynolds number. In addition, the 2D simulation and experimental setup consists of a single layer of cylindrical filaments compared to commercial spacers with two layers of filaments arranged perpendicularly on top of each other. Thus, the flow patterns generated may not be similar to flow patterns caused by commercial spacers.

In feed spacers, the crossing angle or mesh angle refers to the angle created by the crossing of filaments of the top and bottom layers of the spacer. Feed attack angle on the other hand refers to the angle produced between the mean bulk feed

flow direction and the orientation of the feed spacers. The manipulation of these two parameters can have considerable effects on the flow patterns in a spacer filled channel. Lau, et al. (2009) studied the hydrodynamics of the flow induced by spacers of commercial cylindrical filaments by varying its mesh angle and fluid attack angle using the same feed conditions in Lau, et al. (2010). Several different combinations of mesh and feed attack angle are modelled and simulated in 3D in order to optimise the feed spacers in terms of concentration polarisation factor and specific power consumption. In the study, it was found that commercial feed spacers with a mesh angle of 120° and feed attack angle of 30° is the optimal combination in terms of lowest concentration polarisation factor at a specific power consumption. However, this particular combination in a feed spacer was also shown to be the least optimal when high feed Reynolds number is encountered as it generated the highest specific power consumption compared to other combinations.

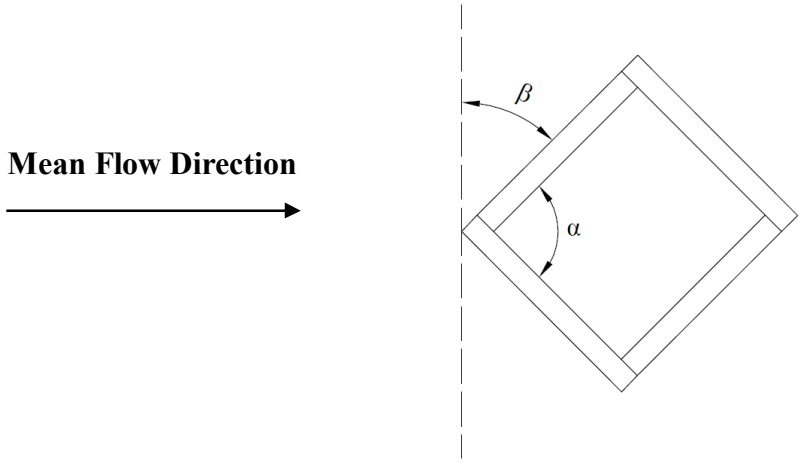

Figure 2.7: Mesh Angle, α and Feed Attack Angle, β

A similar result was obtained by Li, et al. (2002a) as commercial feed spacers were analysed through simulation methods using different mesh and feed attack angles as well as different mesh length ratio. The obtained results agrees with the previously discussed study as the optimal feed spacer was shown to be the one with a mesh angle of 120° and feed attack angle of 30°. In addition, the optimality of the feed spacer in this study is based on the highest value of Sherwood number and a dimensionless power number which is a function of specific power consumption, feed density and viscosity and filament height (Li, et al., 2002a). This shows that the optimal feed spacer is not only most effective in reducing concentration polarisation

but efficient in terms of mass transfer as well. This result was further confirmed experimentally by Li, et al. (2002b). However, the result may be slightly inaccurate as both studies did not test for filaments arranged with a mesh length ratio of 3 as done by Lau, et al. (2009). In terms of mesh length ratio, Li, et al. (2002a) found that a mesh length ratio of 4 is optimal. Also, in the experiment setup, both studies utilised a different feed solution. Lau, et al. (2009) used a feed solution consisting of water and $CuSO_4$ while Li, et al. (2002b) used an aqueous solution of KNO_3, $K_3[Fe(CN)_6]$ and $K_4[Fe(CN)_6]$ with concentration of 0.5 M, 0.001 M and 0.005 M respectively. Therefore, certain aspects of the results might not agree with each other but it can be stated with sufficient confidence that the optimal mesh and feed attack angle of commercial feed spacers are 120° and 30° respectively.

CHAPTER 3

METHODOLOGY

3.1 Channel Geometry and Design

Four different rectangular channels each with equal length and width of 7 mm and a height of 1 mm were designed. Each channel contains cylindrical spacer filaments with a diameter of 0.5 mm placed 3 mm apart from each other. The flow attack angle, β which is the angle of orientation of the spacer filaments with respect to the base edge of the channels i.e. the *x*-*y* plane, were varied from 0° to 15°, 30° and 45°. This is to simulate the different flow attack angles on the spacer filaments. Besides the main spacer-filled channel, an empty channel of length and width of 10 mm by 7 mm was added to the inlet of the spacer-filled channel. This allows for the entering fluid to achieve a fully developed flow profile before entering the spacer filled channel. Besides that, another empty channel of length and width of 12 mm by 7 mm was connected to the outlet of the spacer-filled channel. This is to provide a sufficient exit length for the fluid in order to prevent a reversed flow from occurring in the channel. Figures 3.1 to 3.4 illustrates the design and dimensions of the four spacer channels. The fluid enters the channel from the *x*-*y* plane surface on the far upper right of the channel and flow along the *z*-direction until it exits the channel from the lower-left *x*-*y* plane surface of the channel. All geometries are drawn using DesignModeler accessed through ANSYS Workbench 15.0.

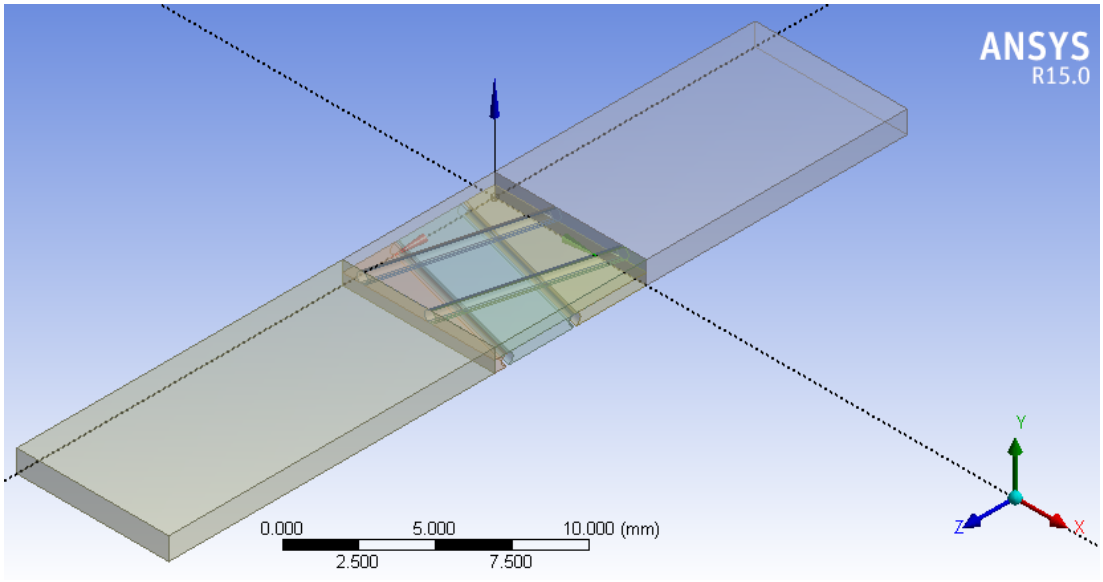

Figure 3.1: Channel Filled with Spacers in 15° Orientation Flow Attack Angle

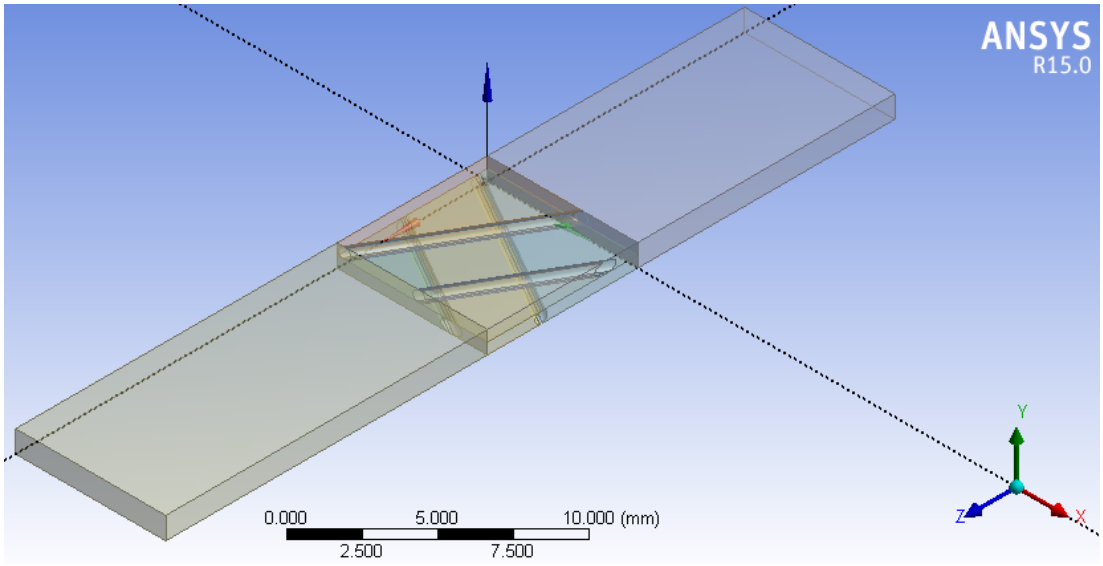

Figure 3.2: Channel Filled with Spacers in 30° Orientation Flow Attack Angle

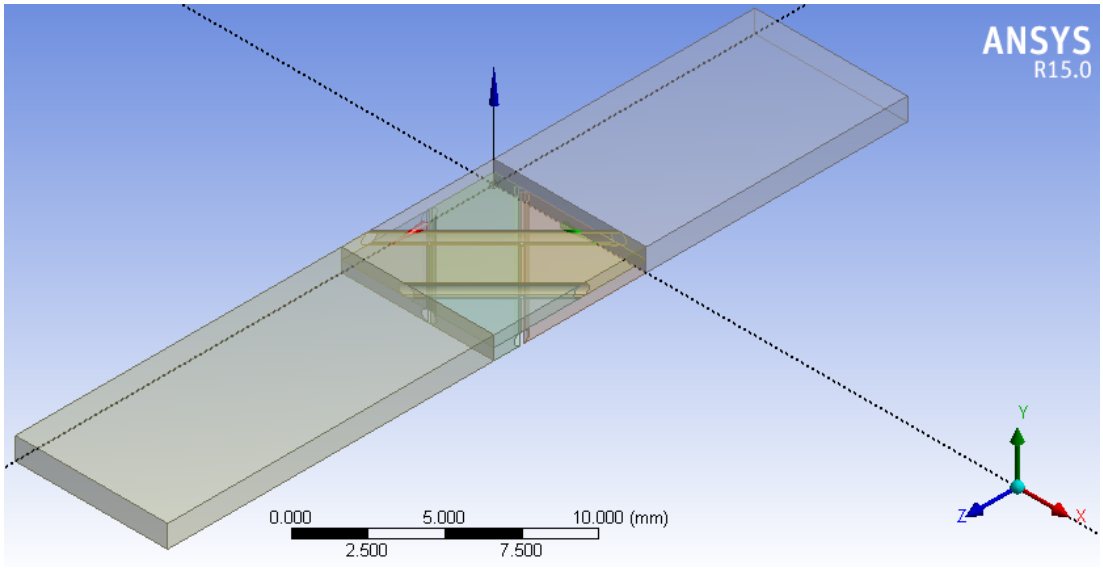

Figure 3.3: Channel Filled with Spacers in 45° Orientation Flow Attack Angle

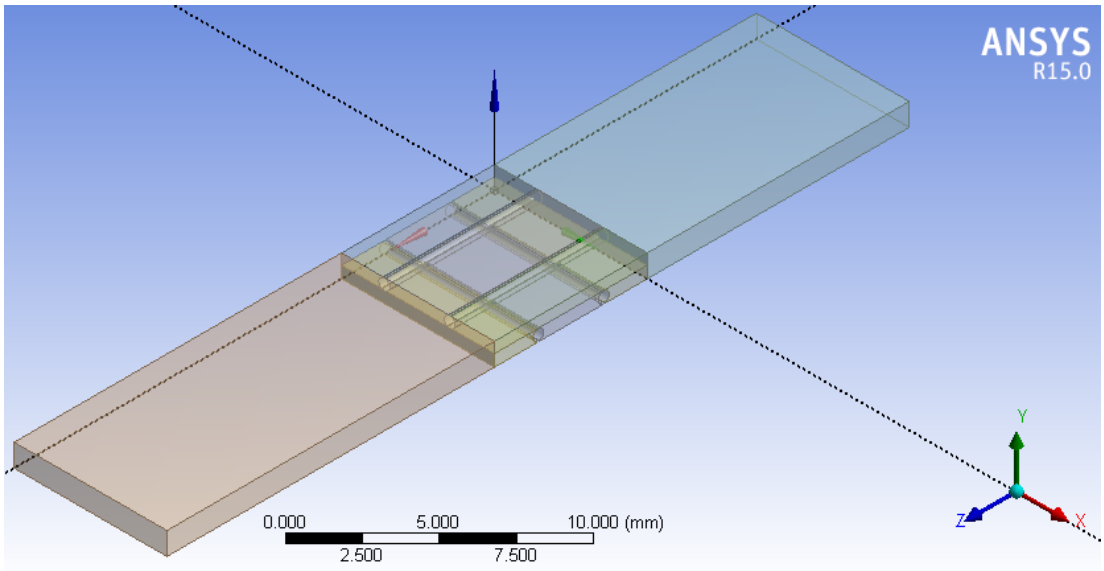

Figure 3.4: Channel Filled with Spacers in 90° Orientation Flow Attack Angle

3.2 Meshing

The mesh of the geometry was setup and generated using Meshing accessed through ANSYS Workbench 15.0. Under the main mesh settings, the physics preference is set to CFD as the fluid flow through the geometry will be analysed using Fluent. Advance size function was turned on for curvature to account for the curved

geometry of the spacer filaments. The relevance centre was set to fine high smoothing, slow transition and fine span angle centre. Also, automatic mesh based defeaturing was turned on to remove potential sliver cells that contributes to the mesh skewness.

The mesh was generated in two parts each using different meshing methods. The first part generates the mesh for the spacer filled channel while the second part generates the mesh for the entrance and exit empty channels adjacent to the spacer filled channel. Due to the complicated internal surface of the spacer filled channel making it non-sweepable nor mappable, a patch independent tetrahedron method was used to generate a mesh of pure tetrahedral elements in the spacer filled channel. This options allows further refinement to be made near the curved region of the channel as well as additional mesh based defeaturing. As such, the refinement was set on curvature and mesh based defeaturing as well as smooth transition were turned on.

As for the adjacent empty channels which serves as an entrance and exit lengths respectively, a general automatic method is used with the default mesh settings. The mesh quality in these regions are irrelevant as their flow patterns will not be analysed in this report. Note that it is important to monitor the statistics of the mesh in order to ensure a sufficient mesh quality. The two important mesh criteria to be met are the mesh skewness and the orthogonal criteria. A skewness value of less than 0.90 and orthogonal quality as low as 0.1 is acceptable. Also done in the meshing stage is the creation of named selections for the geometry. In all the geometries, only the channel inlet and channel outlet were specified while other surfaces were assumed as walls.

3.3 Setup

ANSYS Fluent v15.0 was used to simulate a flow through the spacer filled channel geometry. A pressure-based solver is used to analyse the steady state condition of the fluid flow. The effects of gravity was ignored and velocity formulation was set to relative. The viscous laminar model was used to simulate the flow as the fluid Reynolds number tested is relatively low. Water with a density of 998.2 kg/m^3 and a viscosity of 0.001003 kg/(m.s) was selected as the fluid used in the flow. Throughout the simulation, water is assumed to be a newtonian fluid and no-slip conditions applies to the boundaries (inner walls) of the channel.

For the geometry's boundary conditions, the channel inlet of the geometry was defined as a velocity inlet. Here, the velocity of the flow was varied by manipulating the flows Reynolds number, *Re*. These two parameters were related using the following equation.

$$Re = \frac{\rho V h}{\mu} \tag{3.1}$$

Rearranging,

$$V = \frac{\mu Re}{\rho h} \tag{3.2}$$

where,
V is the mean fluid velocity,
μ is the fluid viscosity,
ρ is the fluid density, and
h is the channel height,

In this study, the Reynolds number was varied from 100 to 500 with a step increment of 100 i.e. 100, 200, 300, 400 and 500. Knowing that the water's viscosity and density as well as channel height are 0.001003 kg/(m.s), 998.2 kg/m^3 and 1 mm respectively, the fluid velocity, V can be calculated. As an example, the fluid velocity when its Reynolds number is 100 was calculated as follows.

$$V = \frac{0.001003(100)}{998.2(1\times10^{-3})} \tag{3.3}$$

$$V = 0.0980 \text{ m/s} \tag{3.4}$$

Using the above approach, the fluid velocity for Reynolds number 200, 300, 400 and 500 were calculated and tabulated in Table 3.1. The channel outlet was set to a pressure outlet and all values were set to be computed using the inlet velocity as a reference value.

Table 3.1: Fluid Velocity of Different Reynolds Number

Feed Reynolds Number	100	200	300	400	500
Feed Velocity (m/s)	0.0980	0.1961	0.2941	0.3921	0.4902

3.4 Solution

The Semi-Implicit Method for Pressure-Linked Equations (SIMPLE) scheme was chosen as a solution method for all the simulations performed. As for the spatial discretisation method, the gradient was discretised based on Green-Gauss nodes which is recommended for a non-uniform tetrahedral mesh. Pressure was discretised using Pressure Stagerring Option (PRESTO!) method as the geometry is highly curved while the momentum was discretised using the second order upwind method to obtain second order accuracy. The under relaxation factors (URF) were kept at the default settings where the pressure, density, body forces and momentum's URF were set to 0.3, 1.0, 1.0 and 0.7 respectively. Initialisation of the solution was done from the channel inlet and the solution was deemed to have converged once the global scaled residual values of the continuity equation falls below 1×10^{-3} and the x, y and z velocity falls below 1×10^{-4}. 5000 iterations was set for each simulation run.

3.5 Results

Data were obtained from a sampling line positioned at the centre of the main spacer-filled channel which contains 701 sampling points in CFD-Post. The type of data obtained include velocity, pressure, shear stress and vortices formed. Graphs of velocity against displacement (position) and pressure drop per unit length against fluid Reynold's number were plotted and compared between different geometries and fluid velocity values. Visual representations of wall shear stress and vortices formed were also compared in the same manner.

3.6 Mesh Independence

In CFD simulations or any simulations in general, the accuracy of the results obtained depends on the mesh quality. By changing the mesh quality, the results obtained may vary significantly even though all other simulation conditions are fixed. Thus, a mesh independence test must be performed for all the geometries used in the simulation. The idea of the test is to repeat the same simulation using increasingly finer meshes. The mesh is usually refined by increasing the number of elements or cells in the mesh. The results are then compared and analysed by taking the average percentage difference between the values of each set of data. If the percentage difference is less than the acceptable criterion, the results are said to be unaffected and hence independent of the mesh quality.

CHAPTER 4

RESULTS AND DISCUSSION

4.1 Mesh Independence Analysis

Since four different geometries are tested in this study, the mesh independence test was performed for each of the geometry by monitoring the average percentage difference between the fluid velocity across the spacer filled channel. The velocity was set to 0.4902 m/s i.e. the velocity of the fluid when the Reynolds number is 500. The mesh quality was refined by increasing the number of cells and the average percentage difference of the velocities obtained from the sampling line were compared between the finer and the coarser mesh. The results are shown in Table 4.1 and the fluid velocity across the centre of each spacer filled channel are plotted in Figures 4.1, 4.2, 4.3 and 4.4. The vertical dotted lines in said figures represent the position of the spacer filaments in the channel.

Based on the average percentage difference calculated, it can be observed that increasing the number of cells, Nc to more than 850010, 1124538, 965018 and 581525 cells for channels filled with 15°, 30°, 45° and 90° spacer filaments respectively, the average percentage difference of the velocity values are less than three percent. Therefore, the results produced by the meshes with said number of cells were assumed to be mesh independent.

Table 4.1: Number of Mesh Cells and Average Percentage Difference in Fluid Velocity of Each Channel Geometry

Geometry	Number of Cells, Nc	Average Percentage Difference (%)
15° Spacers Filaments	790787	-
	850010	5.0975
	917936	2.4510
	1041723	1.2456
30° Spacers Filaments	860187	-
	965018	9.6621
	1124538	5.9356
	1200205	2.6315
45° Spacers Filaments	697546	-
	862767	9.5987
	965018	6.1032
	1128312	2.5056
90° Spacers Filaments	296050	-
	478309	9.6857
	581525	5.8069
	685752	2.6374

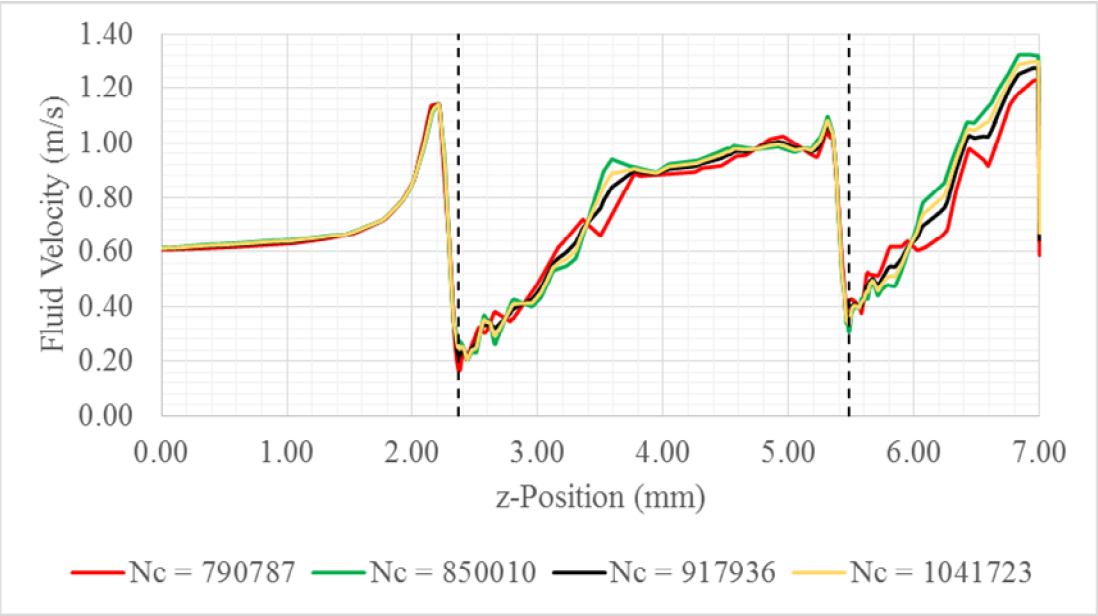

Figure 4.1: Fluid Velocity against *z*-Position in 15° Spacer Filaments Channel

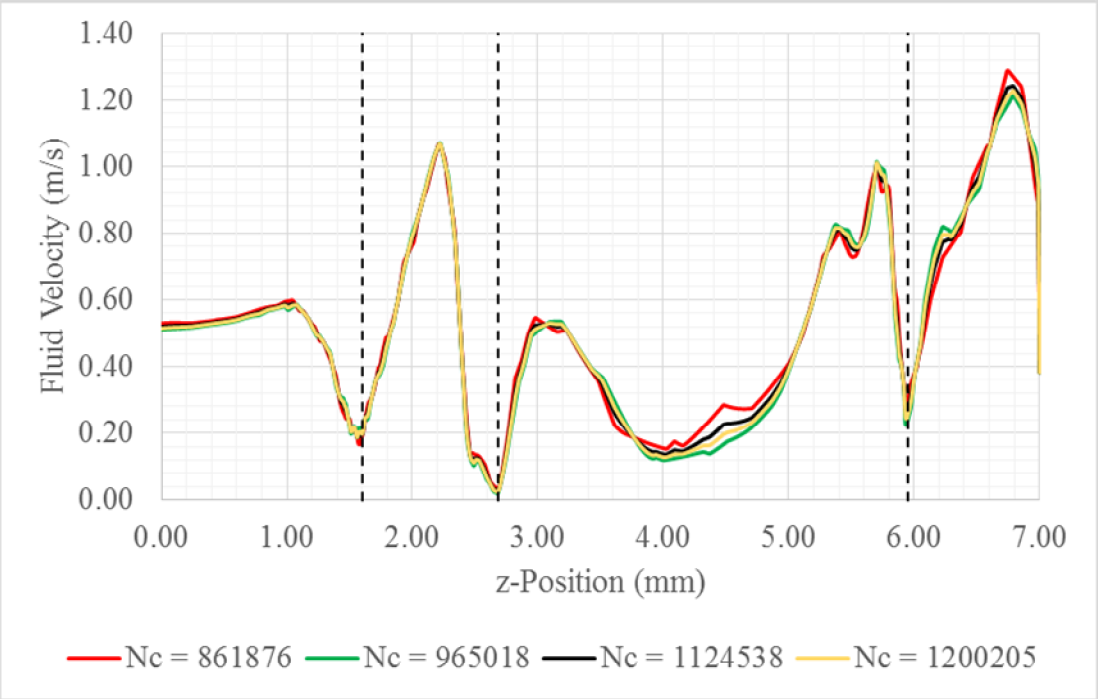

Figure 4.2: Fluid Velocity against z-Position in 30° Spacer Filaments Channel

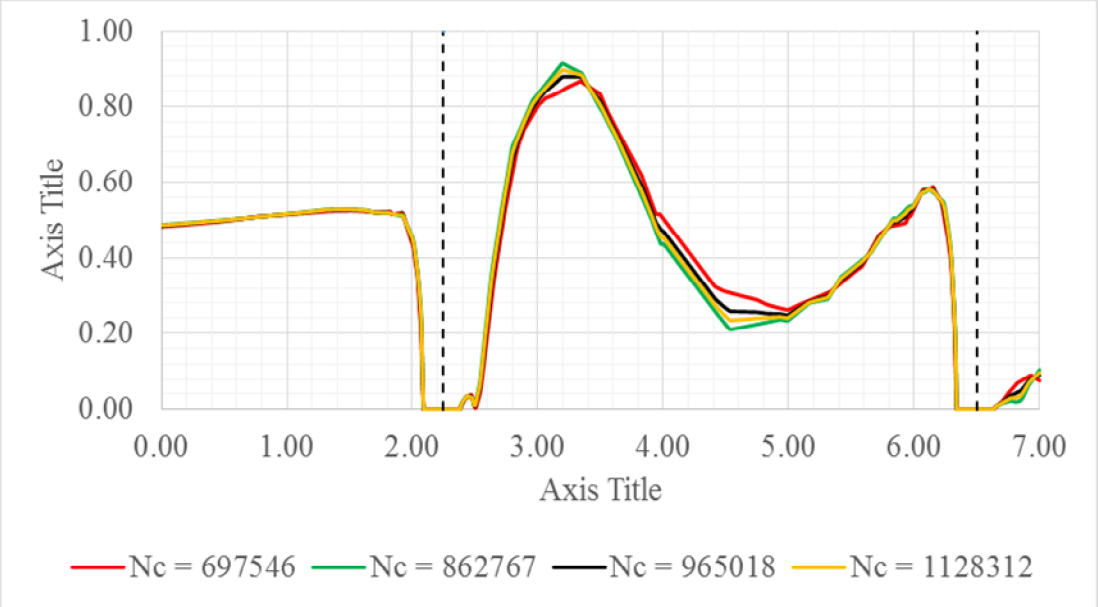

Figure 4.3: Fluid Velocity against z-Position in 45° Spacer Filaments Channel

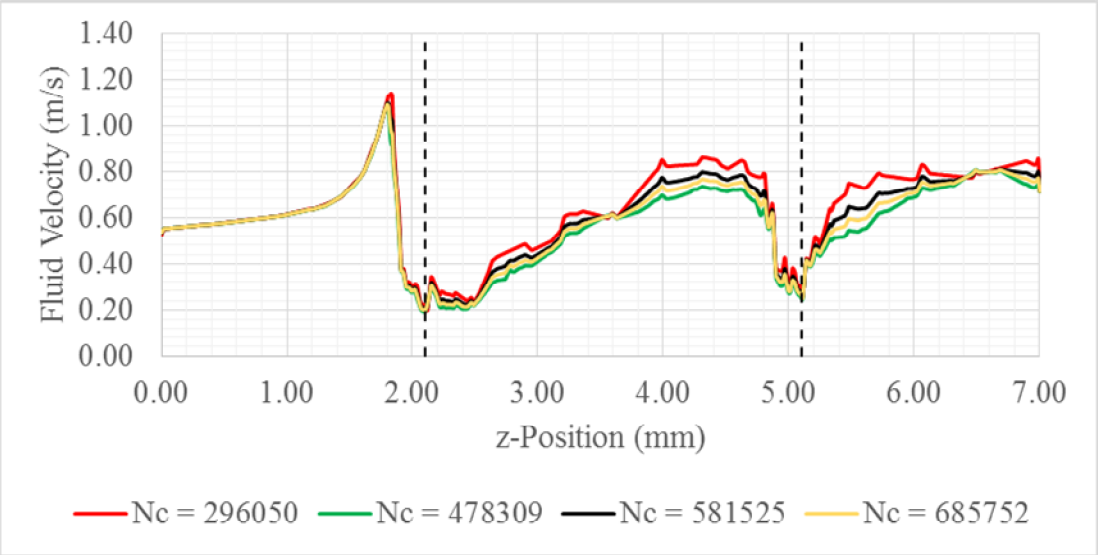

Figure 4.4: Fluid Velocity against z-Position in 90° Spacer Filaments Channel

4.2 Effect of Reynolds Number and Flow Attack Angles on Fluid Velocities Across the Spacer-Filled Channel

The first parameter analysed was the trend of the fluid velocity as it travels across the spacer-filled channel with the same flow attack angle. Five velocity values were tested for each geometry which was varied based on the fluid's Reynolds number in the range of 100 to 500 with an increment of 100 between the range i.e. 100, 200, 300, 400 and 500. The results were analysed by comparing the trends in fluid velocities of different Reynolds number flowing across the spacer-filled channel with the same flow attack angle as well as the trends in fluid velocities of the same Reynolds number flowing across spacer-filled channels with different flow attack angles. Figures 4.5, 4.6, 4.7 and 4.8 shows the trends of the different velocities tested in each spacer-filled channel that provides different flow attack angles.

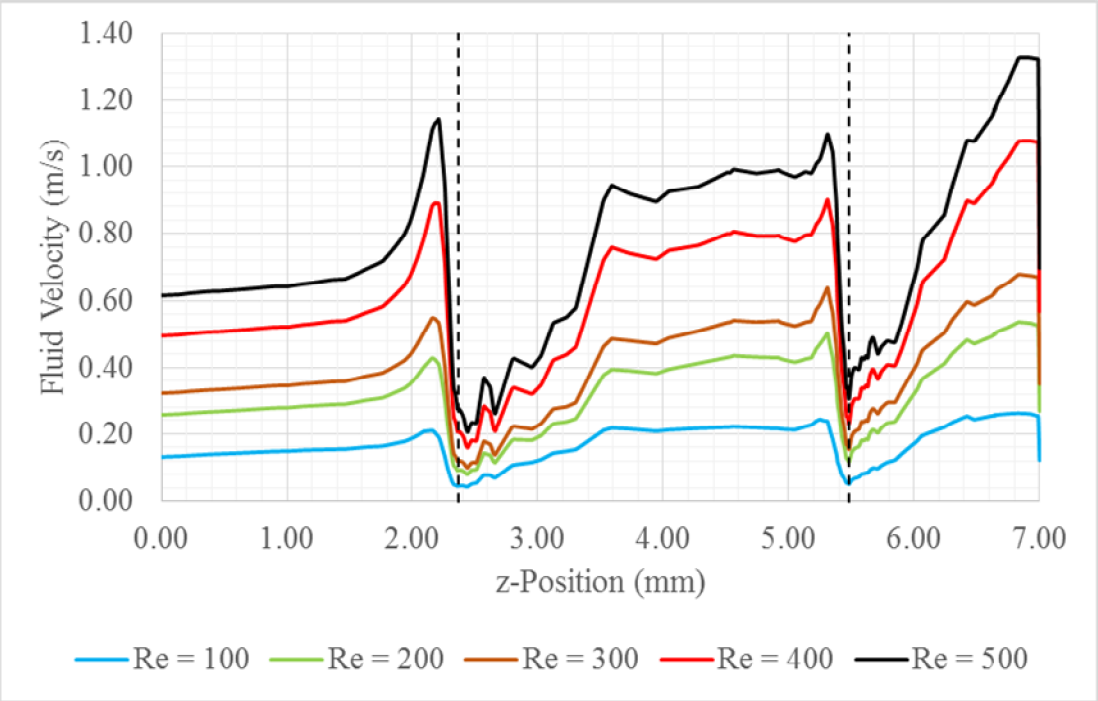

Figure 4.5: Fluid Velocity against z-Position in 15° Flow Attack Angle

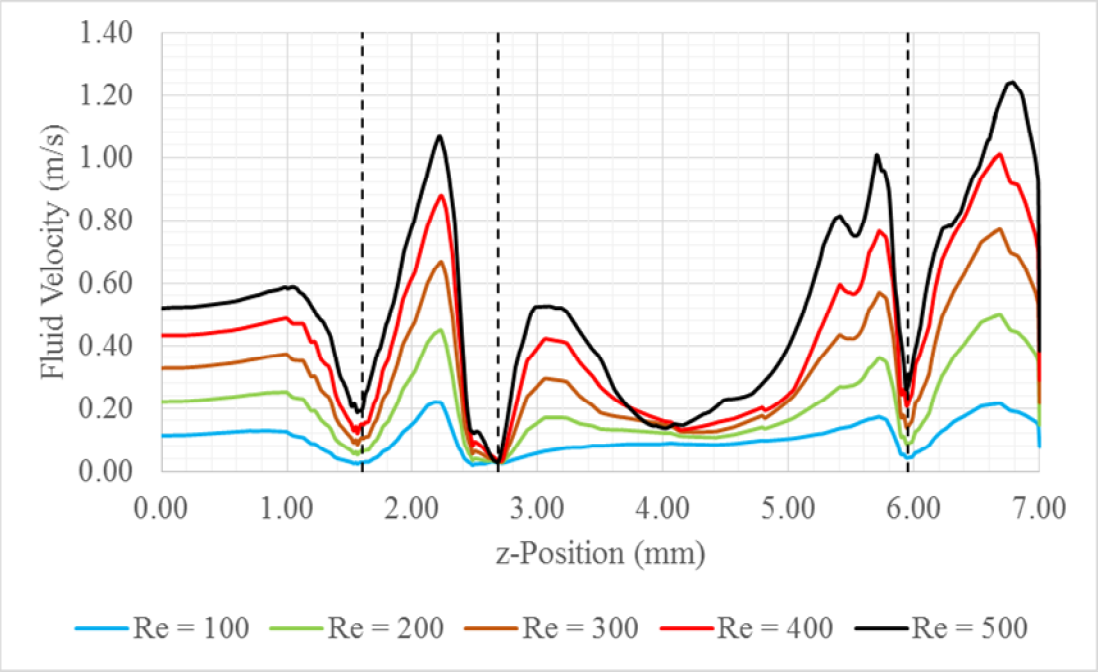

Figure 4.6: Fluid Velocity against z-Position in 30° Flow Attack Angle

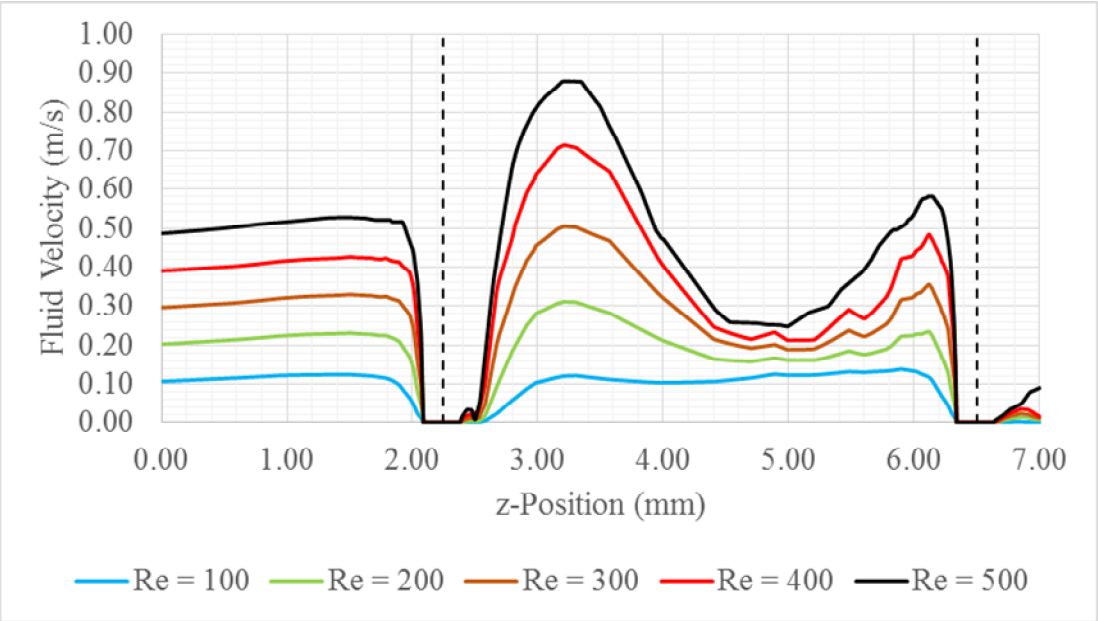

Figure 4.7: Varying Fluid Reynolds Number in 45° Spacer Channel

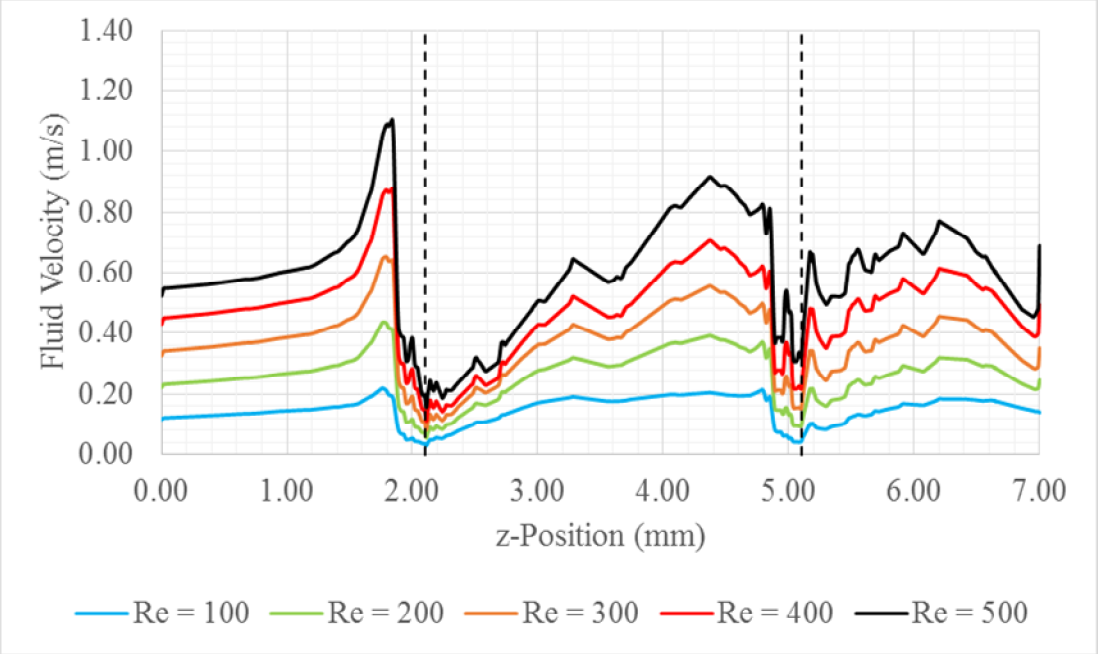

Figure 4.8: Varying Fluid Reynolds Number in 90° Spacer Channel

4.2.1 Fluid Velocities of Varying Reynolds Number with Constant Flow Attack Angle

Initially, it was expected to observe a difference in the trend of fluid velocities across the spacer filled channel as the Reynolds number is increased. However, there was no observable difference in the velocity trends aside from the trivially higher velocity values exhibited by fluid with higher Reynolds number. This shows that the fluid's Reynolds number does not affect the trends in the fluid's velocities along the spacer-filled channel. Instead, the fluid velocity's trends is more dependent on the inner geometry of the spacer filled channel, in this case the flow attack angle. This is evident from the different shapes of fluid velocity against z-Position curves produced using spacer-filled channels with different flow attack angles. Hence, it was found that comparing the flow of fluids with a constant Reynolds number flowing in channels of different flow attack angle will be more meaningful and informative.

4.2.2 Fluid Velocities of Constant Reynolds Number and Varying Flow Attack Angle

Based on Figures 4.4, 4.5, 4.6 and 4.7, the fluid velocities will drop drastically as the flow comes in contact and hits the spacer filaments. This observation holds true for all the fluid's Reynolds number tested regardless of its flow attack angle. However, it can be observed that the increase in the velocity magnitude after the flow passes through a spacer filament differs with the flow attack angle. Consider the flow with Reynolds number of 500 in the figures 4.4 to 4.7. The fluid velocity immediately after it passes through the first spacer is approximately 0.2 m/s for each flow attack angle except the 45° flow attack angle which has a zero fluid velocity magnitude near the spacer filament region. In the case of fluid with a 15° flow attack angle, the velocity magnitude increased from 0.2 m/s to a maximum of 1.1 m/s, yielding a net increase of 0.9 m/s. Flow attack angle of 30°, 45° and 90° yielded a net increase of 0.9 m/s, 0.7 m/s and 0.7 m/s respectively.

It is important to monitor the fluctuations of flow velocity magnitude as it affects the particle deposition percentage on the spacer filaments as well as the on the membrane. Generally, a higher fluid velocity is desired as it increases the wall shear stress which promotes the dislodging of particles from the membrane surface and hence reduces fouling (Li, et al., 2012). Since the fluid velocity was able to recover its magnitude in each of the flow attack angle tested, an optimal flow attack angle and Reynolds number cannot be decided by solely considering the fluid velocity.

4.3 Effect of Reynolds Number and Flow Attack Angles on Pressure Drop Across Channel

Besides monitoring the trends of fluid velocity in the spacer, it is also important to analyse the fluid's pressure drop across the spacer-filled channel. In an SWM module, the amount of permeate measured as the permeate flux across the membrane depends largely on the fluid pressure on the membrane. A decrease in pressure may lead to an inefficient permeation of certain materials in the feed stream across the membrane and hence creating a concentration gradient of said materials across the SWM module. This phenomenon is also known as concentration polarisation. Hence, it is desired to minimise the pressure drop in the fluid as it flows through the spacer-filled channel of a SWM module. Figure 4.9 shows the relationship between the pressure drop per unit length across the spacer-filled channel of different flow attack angles plotted against the fluid's Reynolds number.

Based on Figure 4.9, it can be seen that the flow attack angle of 90° is superior to the other flow attack angles as it produces the lowest pressure drop values followed by 15°, 45° and 30° flow attack angles. This can be attributed to the uniform arrangement of the spacer filaments as they are arranged either in parallel or perpendicular to the fluid flow. Hence, produces a more uniform flow with less unsteady hydrodynamics and eddies and thus resulting in a low pressure drop. This result is also in agreement with the study done by Lau, et al. (2009) which produced similar pressure drop values. Slight variations between these results and the said study may be due to the different solution methods used during simulation. By

considering the linear coefficient of determination value, R^2, the data shown seems to have a good linear relationship as all the R^2 values are higher than 0.95.

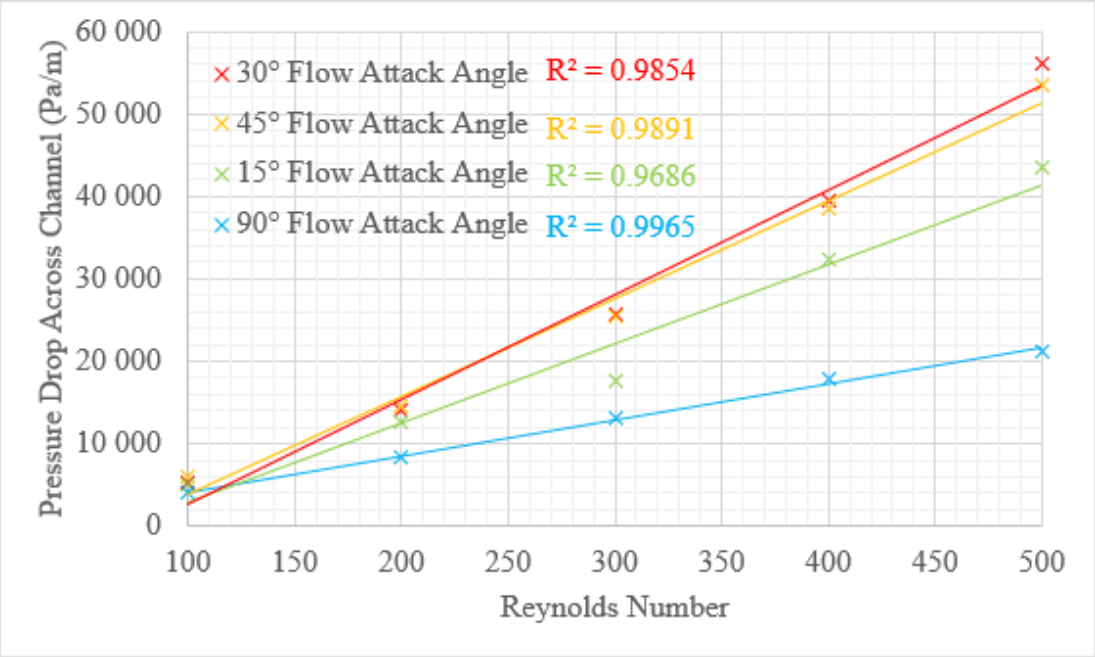

Figure 4.9: Pressure Drop Across Channel against Fluid's Reynolds Number

4.4 Effect of Reynolds Number and Flow Attack Angles on Wall Shear Stress Distribution Across Channel

The distribution of wall shear stress across the spacer-filled channel depends largely on the fluid velocity patterns. While velocity trends can be represented using a single line in a graph as shown in Section 4.1, the wall shear stress distribution is better illustrated using visual representations. Also, it has been shown that wall shear stress data obtained from a 3D model of a spacer-filled channel is more reliable compared to a 2D model as a 3D model accounts for both longitudinal and transverse velocity patterns (Santos, et al., 2007). In the case of wall shear stress, it is desired maximise its magnitude as well as having it distributed in equal concentrations on the top and bottom wall of the channel. Figures 4.10, 4.11, 4.12 and 4.13 shows a graphical representation of the wall shear stress on the top and bottom surface of the channels

with different flow attack angles and fluid Reynolds number. Recall that the fluid flows through the channel along the positive z-direction.

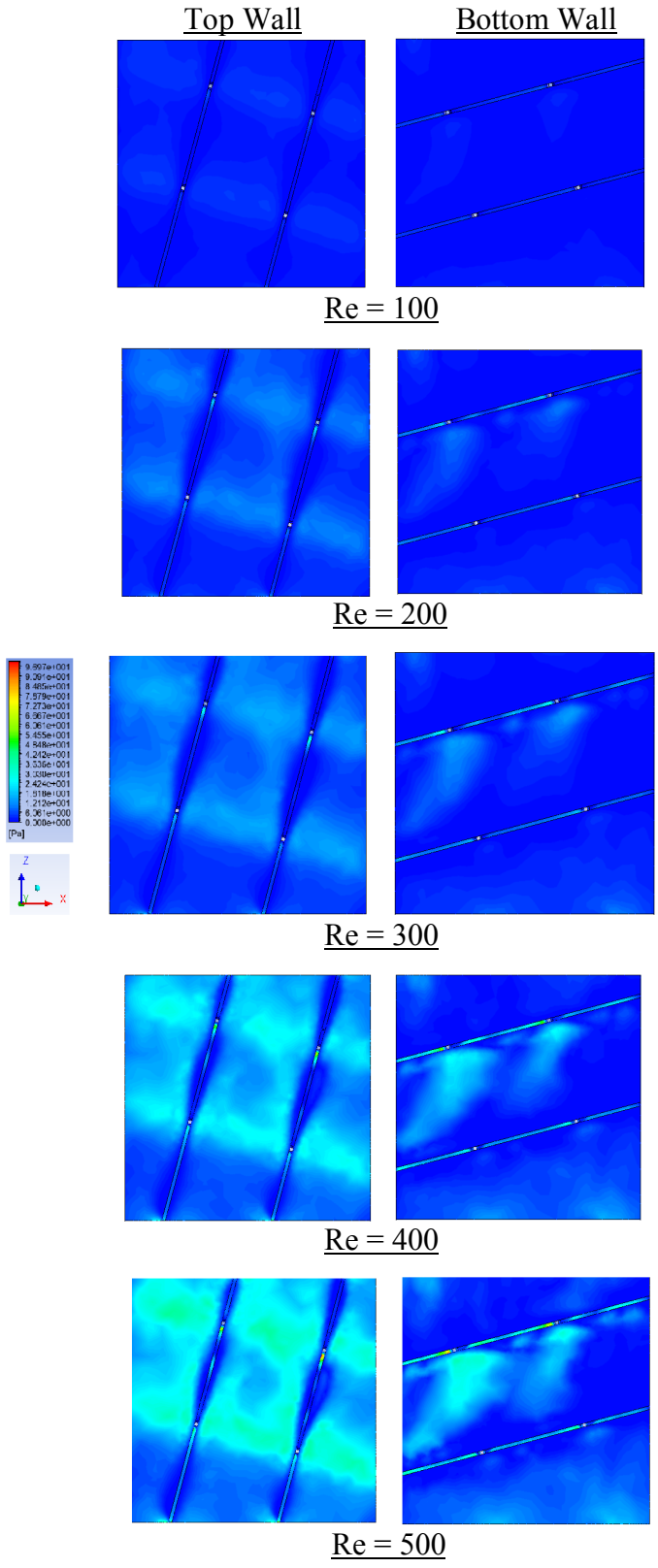

Figure 4.10: Top and Bottom Wall Shear of 15° Flow Attack Angle

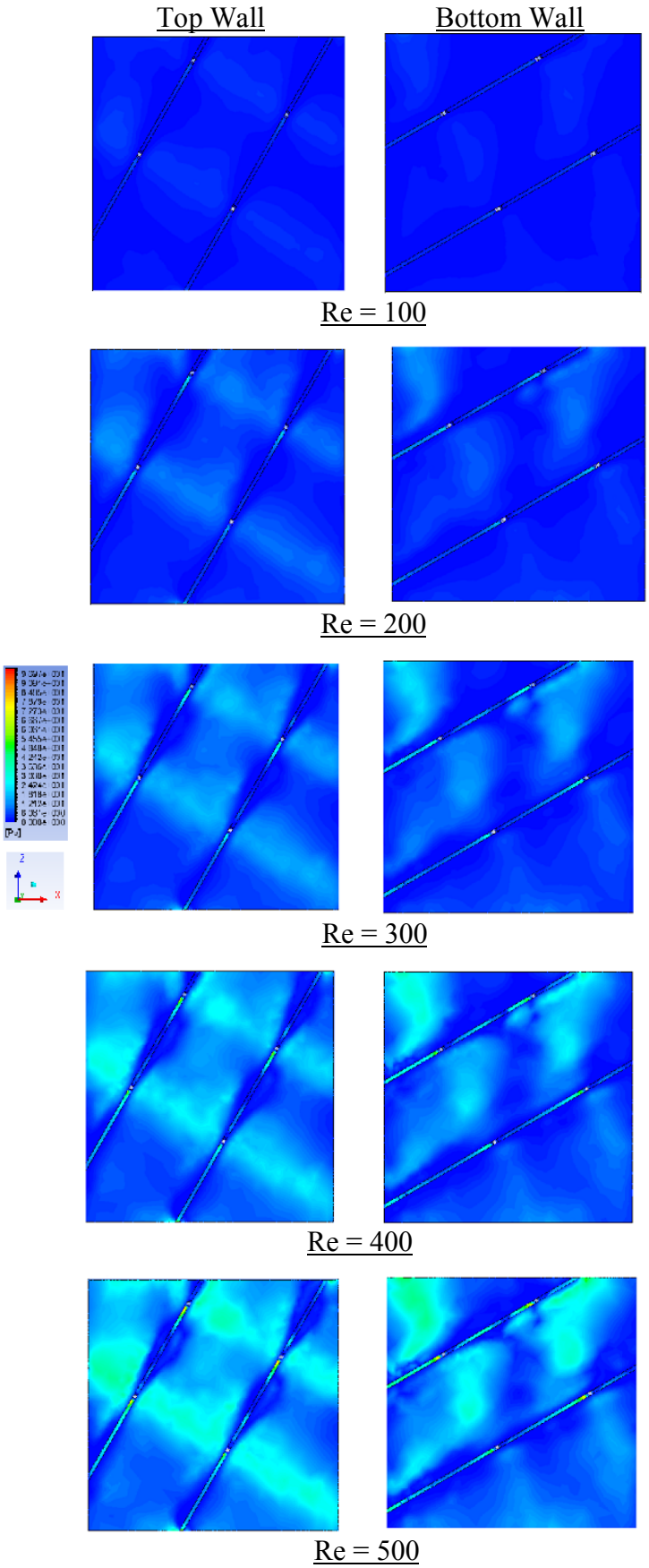

Figure 4.11: Top and Bottom Wall Shear of 30° Flow Attack Angle

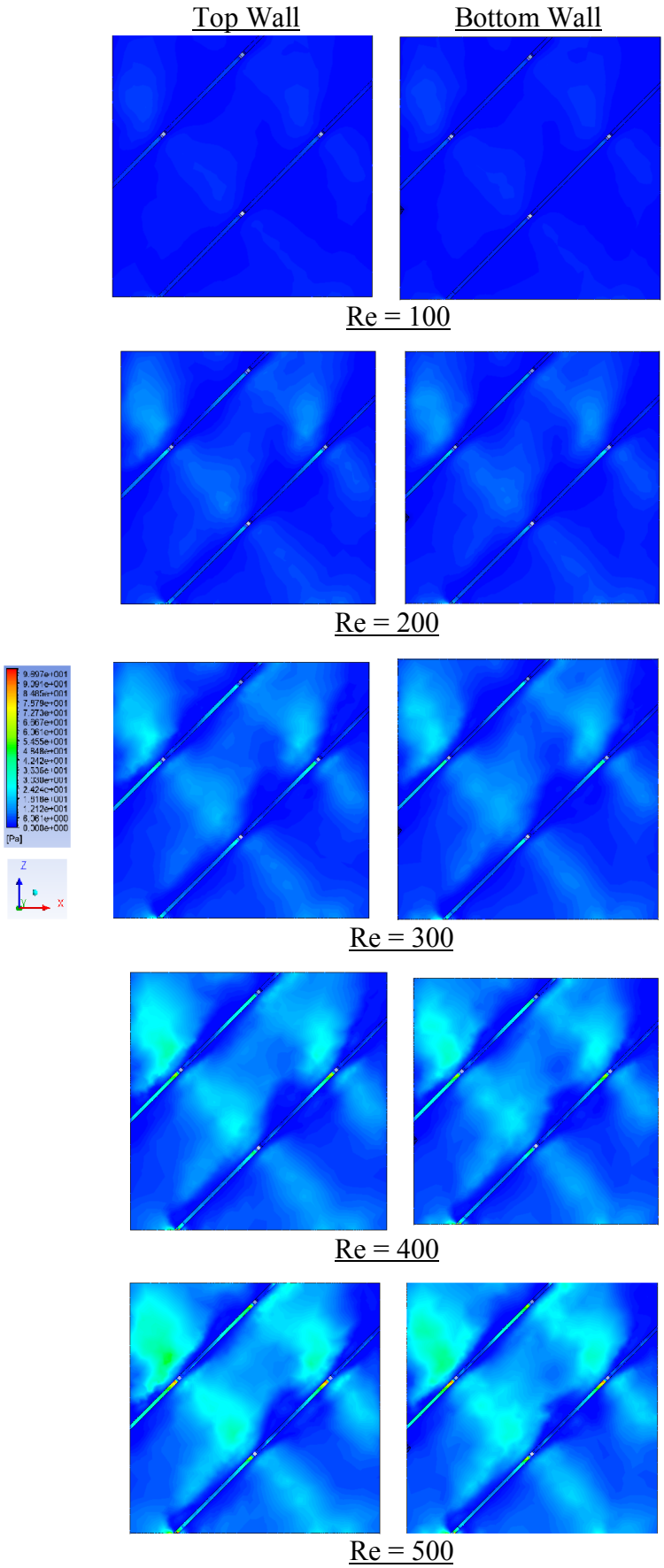

Figure 4.12: Top and Bottom Wall Shear of 45° Flow Attack Angle

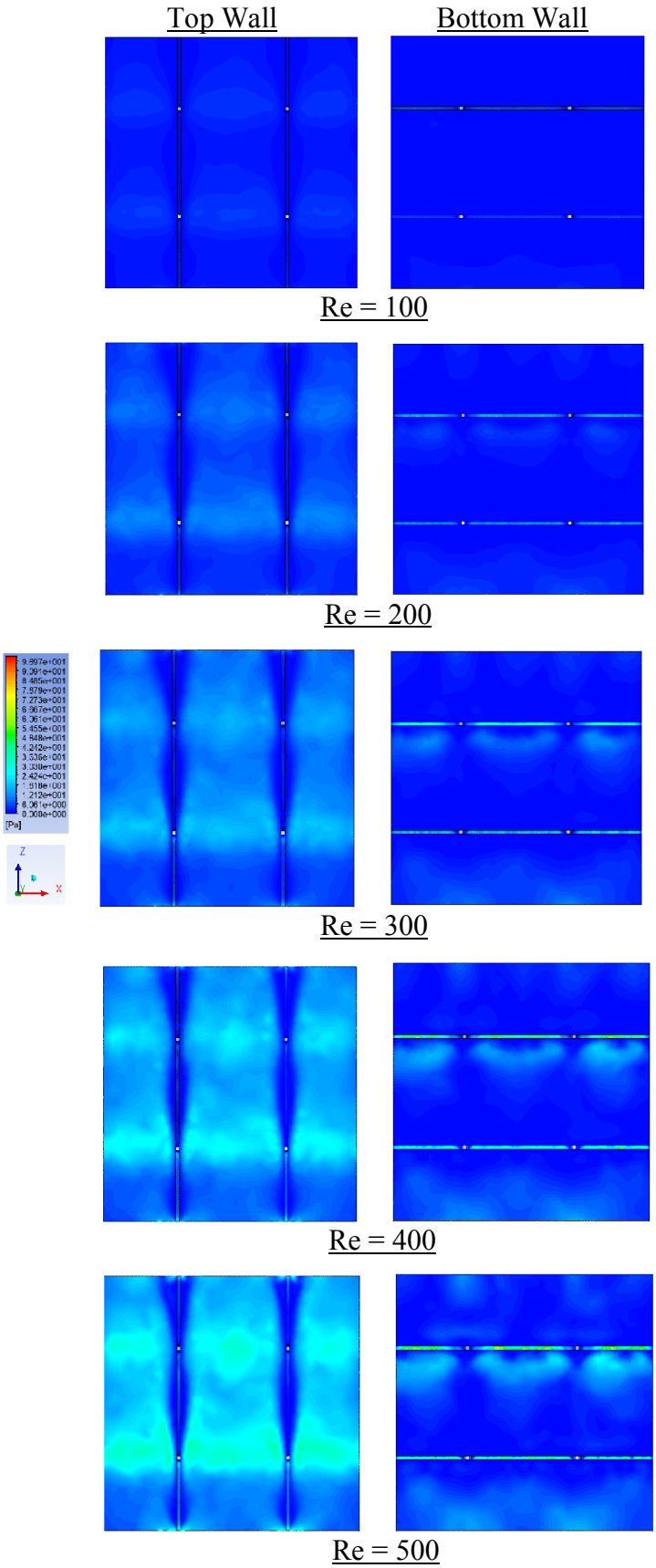

Figure 4.13: Top and Bottom Wall Shear of 90° Flow Attack Angle

Although the fluid velocity patterns varied considerably with different flow attack angles, the magnitude of the wall shear stress did not show any significant changes as the flow attack angle was changed. Instead, the shear stress magnitude seemed to be dependent on only the magnitude of the Reynolds number. For instance, in cases of low Reynolds number i.e. 100 and 200, the shear stress magnitude was observed to be very small and insignificant while fluid Reynolds number of 300 to 500 produced notable shear stress value. This observation showed that the fluid velocity plays an important role in inducing wall shear stress.

However, the changes in the attack angle affected the distribution of the wall shear stress. Consider the fluid with Reynolds number of 500 of each of the flow attack angle tested. While the fluid was able to produce similar magnitudes of wall shear stress in each flow attack angle, the area of concentration of the stress was shown to be comparably different. For instance, the wall shear stress in the 90° flow attack angle channel was concentrated more on the top wall compared to the bottom wall which has a much lower concentration, while the 45° flow attack angle exhibited almost equal concentrations of wall shear stress on both the top and bottom wall. The wall shear stress patterns in 30° and 15° flow attack angle yielded a similar observation to the 45° and 90° flow attack angle respectively. As the fluid flows across the channel with a 90° flow attack angle, it was obstructed mostly by the spacer filaments of the bottom half of the channel which were perpendicular to the flow while less obstructions were encountered on the top part of the channel as the spacer filaments were placed parallel to the flow. This caused most of the fluid to be diverted upwards and hence inducing a high wall shear stress on the top wall. In the case of the 45° flow attack angle, equal amount of obstruction was encountered by the flow in top and bottom part of the channel causing an equal distribution of wall shear stress. Therefore, in terms of wall shear stress distribution, spacers with 45° attack angle outperforms the other flow attack angle as it yielded the most desired equal stress concentration on top and bottom part of the wall.

4.5 Effect of Reynolds number and Flow Attack Angle on Vortices Formation in Channel

One of the main functions of the spacer filaments in the spacer-filled channel besides providing mechanical support to the membrane layers is to induce turbulent and unsteady hydrodynamics in the feed flow. The magnitude of unsteadiness in the hydrodynamics of the flow can be judged by visualising the amount of vortices or eddies form in the flow. Similar to the case of wall shear stress, it is desired to maximise the amount of vortices as well as having equal concentration of vortices on both the top and bottom walls of the channel. Figures 4.14, 4.15, 4.16 and 4.17 shows the streamlines of fluid of different Reynolds number and flow attack angle at the centre of the spacer-filled channel. Recall that the fluid flows in the across the channel along the positive z-direction.

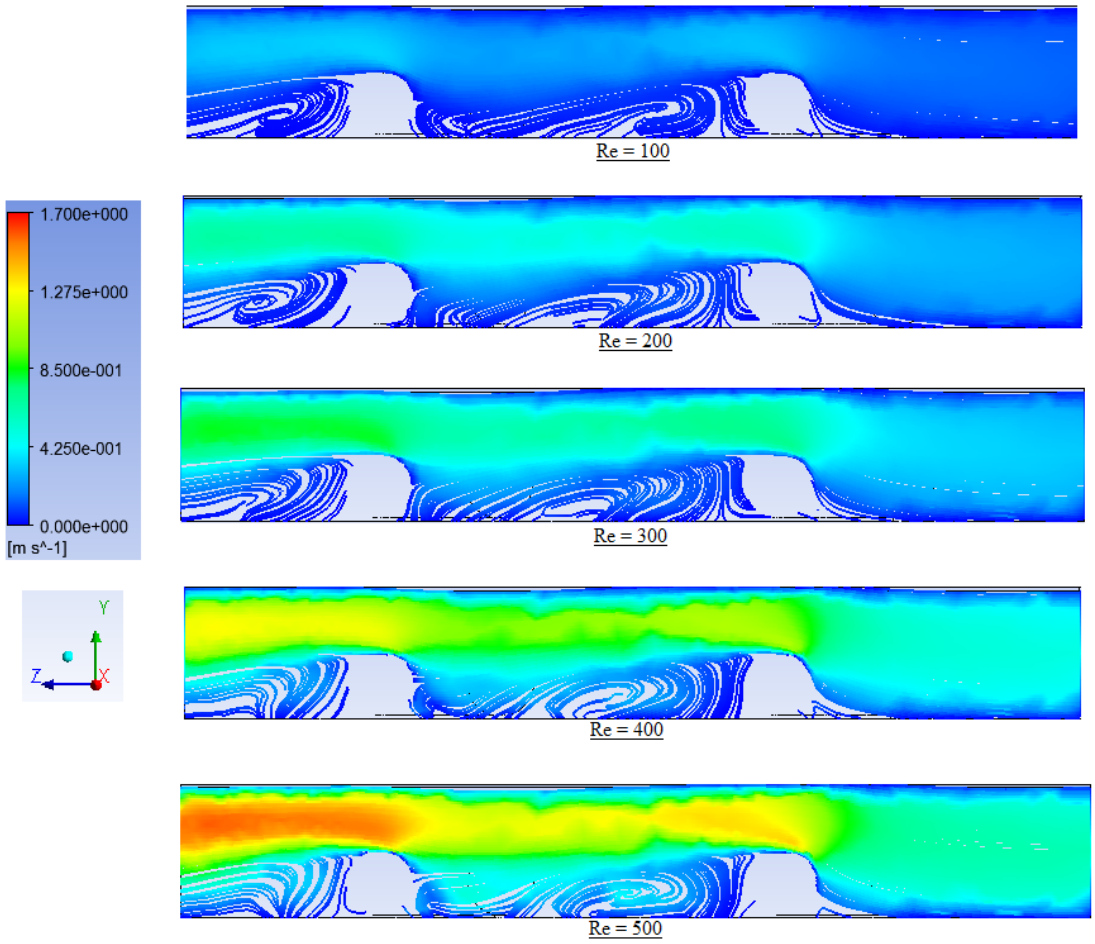

Figure 4.14: Streamlines of Fluid of Different Reynolds Number of 15° Flow Attack Angle

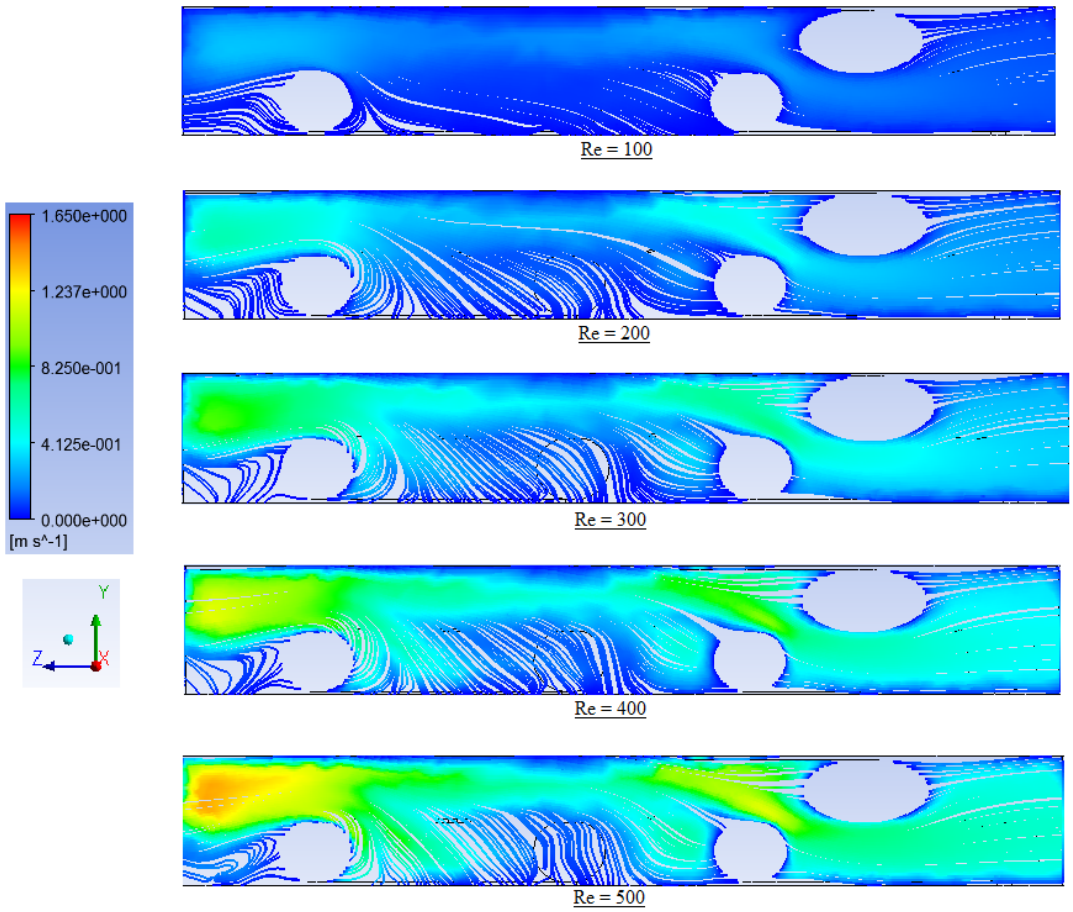

Figure 4.15: Streamlines of Fluid of Different Reynolds Number of 30° Flow Attack Angle

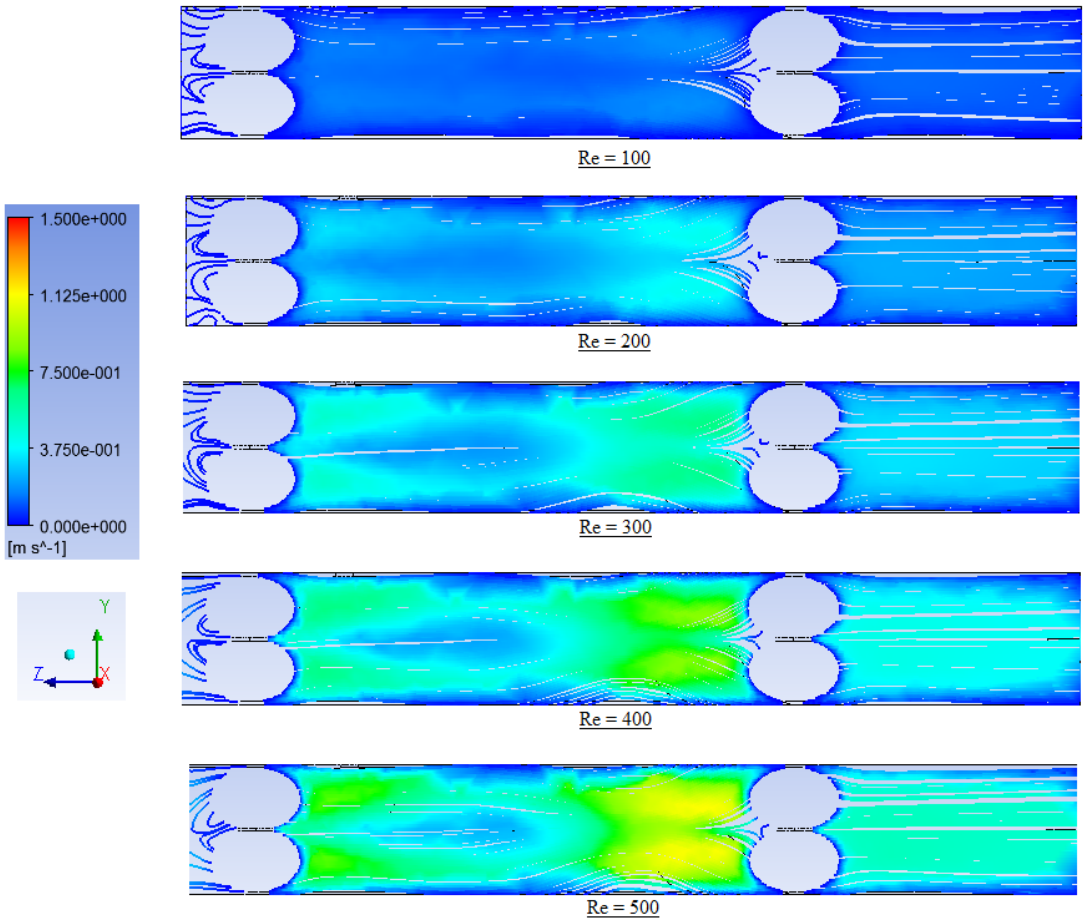

Figure 4.16: Streamlines of Fluid of Different Reynolds Number of 45° Flow Attack Angle

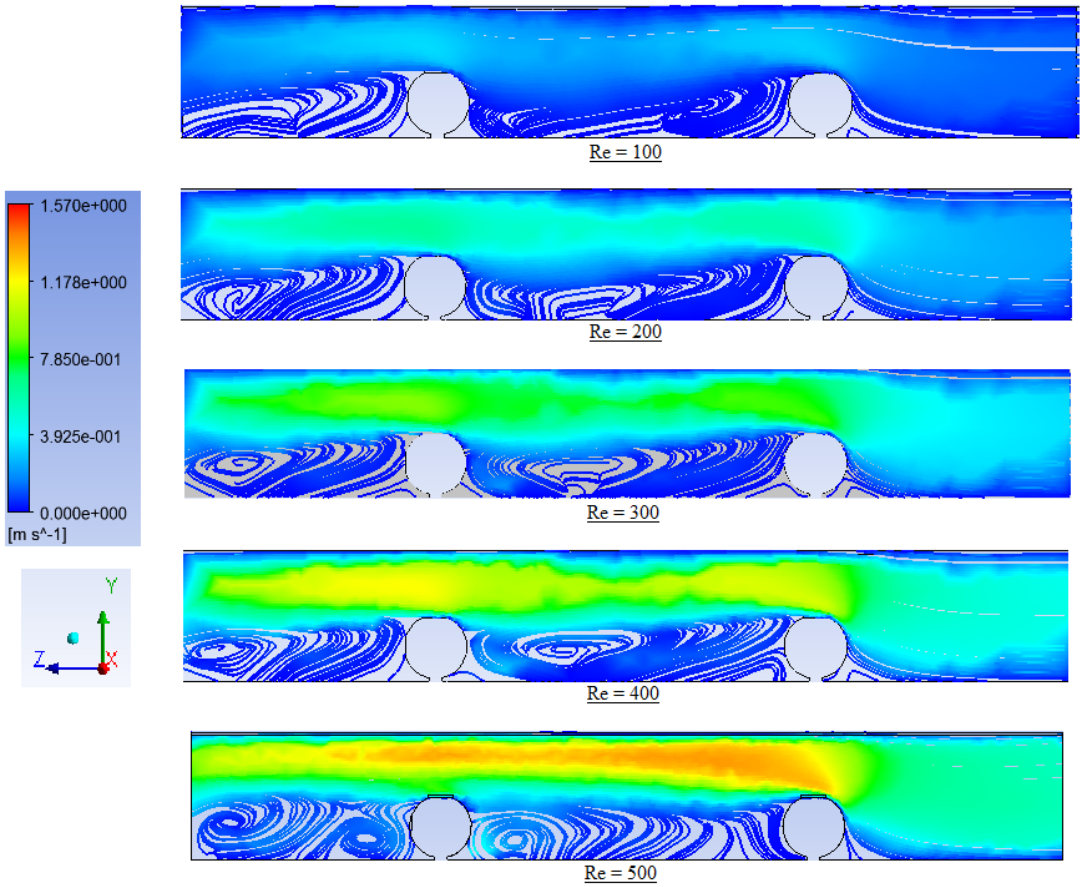

Figure 4.17: Streamlines of Fluid of Different Reynolds Number of 90° Flow Attack Angle

Based on the figures above, it can be seen that in the case of fluids with 15° and 90° flow attack angle, the fluid flow in the top half of the channel were seen to be steady and uniform with vortices tending to occur only in the lower half of the channel. By comparing the vortices formed between fluids of 15° and 90° flow attack angle, it was clear that a larger amount of vortices was formed in 90° flow attack angle. Whereas in the cases of 30° and 45° flow attack angle, the fluid flow tends to fill the entire height of the channel. Although no vortices were observed, the fluid flow in both 30° and 45° flow attack angle exhibited the formation of eddies which also helps in recirculating the flow and thus reducing fouling. Considering the magnitude of the eddies, the 30° flow attack angle produced larger eddies compared to the 45° flow attack angle. Overall, the flow patterns found in 30° flow attack angle channel was the best among all tested as it yielded an unsteady flow and yet was able to fill the entire channel while producing large eddies.

CHAPTER 5

CONCLUSION AND RECOMMENDATIONS

5.1 Conclusion

As a conclusion, the flow patterns of fluid with different Reynolds number as well as flow attack angles were analysed based on their fluid velocity trends, pressure drop, wall shear stress as well as vortices and eddies formation across the spacer-filled channel. In the test of velocity patterns, none of the Reynolds number nor flow attack angle was seen to be better than the other as the fluid velocity was able to recover itself after dropping drastically as it flowed across a spacer filament. In terms of pressure drop where a low value is desired, the flow of 90° attack angle yielded the lowest pressure drop across the channel. However, the fluid with 45° flow attack angle exhibited optimal wall shear stress values as almost equal concentrations were present at the top and bottom channel wall. On the other hand, fluid with 30° flow attack angle flowed with the most unsteady and non-uniform hydrodynamics with large eddies being formed while filling the entire channel. Also, observations on wall shear stress as well as vortices and eddies in flow patterns noted that the fluid must possess a Reynolds number higher than 200 to exhibit reasonable magnitudes of said parameters. As each flow attack angle has their own advantages, it is difficult to conclude and decide on an optimal flow attack angle. However, in the case where a single flow attack angle has to be chosen, the 45° flow attack angle should be the preferred selection as it exhibited balanced wall shear stress on both top and bottom channel wall as well as formation of eddies in its flow pattern despite having a second largest pressure drop value among all the flow attack angle tested.

5.2 Recommendations

It is important to note that the scope of this study is limited and hence needed to be expanded in order to better reflect the actual flow patterns in a SWM module. One method of improving the study is to increase the range of fluid Reynolds number tested. Also, additional parameters such as the permeate flux and specific power consumption can be monitored in order to make a better conclusion on the optimal flow attack angle.

REFERENCES

Ahmad, A. L., Lau, K. K., Abu Bakar, M. Z. and Abd. Shukor, S. R., 2005. Integrated CFD simulation of concentration polarization in narrow membrane channel. *Computers and Chemical Engineering*. 29(2005), pp. 2087–2095.

Ahmad, A. L., Lau, K. K., 2006. Impact of different spacer filaments geometries on 2D unsteady hydrodynamics and concentration polarization in spiral wound membrane channel. *Journal of Membrane Science*. 286(2006), pp. 77–92.

Baker, R. W., 2004. *Membrane Technology and Applications*. 2nd ed. West Sussex, England: John Wiley & Sons.

Dendukuri, D., Karode, S. K. and Kumar, A., 2005. Flow visualization through spacer filled channels by computational fluid dynamics-II: improved feed spacer designs. *Journal of Membrane Science*. 249(2005), pp. 41–49.

Fimbres-Weihs, G. A. and Wiley, D. E., 2010. Review of 3D CFD modelling of flow and mass transfer in narrow spacer-filled channels in membrane modules. *Chemical Engineering and Processing*. 49(2010), pp. 759–781.

Koros, W. J., Ma, Y. H. and Shimidzu. T., 1996. Terminology for membranes and membrane processes. *Pure & Applied Chemistry*. 68(7), pp.1479–1489.

Koutsou, C. P., Yiantsios, S. G. and Karabelas, A. J., 2007. Direct numerical simulation of flow in spacer-filled channels: Effect of spacer geometrical characteristics. *Journal of Membrane Science*. 291(2007), pp. 53–69

Munson, B. R., Okiishi, T. H., Huebsch, W. W. and Rothmayer, A. P., 2013. *Fundamentals of Fluid Mechanics*. 7th ed. Hoboken, NJ: John Wiley & Sons.

Nath, K., 2008. *Membrane Separation Processes*. New Delhi, India: Prentice Hall of India.

Lau, K. K., Abu Bakar, M. Z., Ahmad, A. L. and Murugesan, T., 2009. Feed spacer mesh angle: 3D modelling, simulation and optimization based on unsteady hydrodynamic in spiral wound membrane channel. *Journal of Membrane Science*. 343(2009), pp. 16–33.

Lau, K. K., Abu Bakar, M. Z., Ahmad, A. L. and Murugesan, T., 2010. Effect of Feed Spacer Mesh Length Ratio on Unsteady Hydrodynamics in 2D Spiral Wound Membrane (SWM) Channel. *Industrial & Engineering Chemistry Research*. 49(12) pp. 5834–5845.

Li, F., Meindersma, W., de Haan, A. B. and Reith, T., 2002a. Optimization of commercial net spacers in spiral wound membrane modules. *Journal of Membrane Science*. 208(2002), pp. 289–302.

Li, F., Meindersma, W., de Haan, A. B. and Reith, T., 2002b. Optimization of non-woven spacers by CFD and validation by experiments. *Desalination*. 146(2002) pp. 209–212.

Li, F., Meindersma, W., de Haan, A. B. and Reith, T., 2005. Novel spacers for mass transfer enhancement in membrane separations. *Journal of Membrane Science.* 253(2005) pp. 1–12.

Li, Y. L., Tung, K. L., Chen, Y. S. and Hwang, K. J., 2012. CFD analysis of initial stages of particle deposition in spiral-wound membrane modules. *Desalination.* 287(2012) pp. 200–208.

Santos, J. L. C., Geraldes, V., Velizarov, S. and Crespo, J. G., 2007. Investigations of flow patterns and mass transfer in membrane module channels filled with flow-aligned spacers using computational fluid dynamics (CFD). *Journal of Membrane Science.* 305(2007), 103–117.

Shakaib, M., Hasani, S. M. F. and Mahmood, M., 2007. Study on the effects of spacer geometry in membrane feed channels using three-dimensional computational flow modelling. *Journal of Membrane Science*. 297(2007), pp. 74–89.

Shrivastava, A., Kumar, S. and Cussler, E. L., 2008. Predicting the effect of membrane spacers on mass transfer. *Journal of Membrane Science.* 323(2008), pp. 247–256 .